A semi-analytical model for the behavior of saturated viscoplastic materials containing two populations of voids of different sizes

Jérôme Julien, Mihail Garajeu, Jean-Claude Michel

A semi-analytical model for the behavior of saturated viscoplastic materials containing two populations of voids of different sizes.

Jérôme Julien[a,1], Mihail Gărăjeu[b,*], Jean-Claude Michel[c]

[a] *Électricité de France, Département Matériaux et Mécanique des Composants, Site des Renardières, 77818 Moret-sur-Loing, France*
[b] *Aix-Marseille Université, M2P2/UMR 6181, Faculté des Sciences et Techniques, Av. Escadrille Normandie-Niemen, Case 322, Marseille, F-13397, France*
[c] *Laboratoire de Mécanique et d'Acoustique, CNRS, 31 Chemin Joseph Aiguier, 13402 Marseille Cedex 20, France*

Abstract

This paper presents a micromechanical model for a porous viscoplastic material containing two populations of pressurized voids of different sizes. Three scales are distinguished: the microscopic scale (corresponding to the size of the small voids), the mesoscopic scale (corresponding to the size of the large voids) and the macroscopic scale. It is assumed that the first homogenization step is performed at the microscopic scale, and, at the mesoscopic scale, the matrix is taken to be homogeneous and compressible. At the mesoscopic scale, the second homogenization step, on which the present study focuses, is based on a simplified representative volume element: a hollow sphere containing a pressurized void surrounded by a nonlinear viscoplastic compressible matrix. The nonlinear behavior of the matrix, which is expressed using the results obtained in the first homogenization step, is approached using a modified secant linearization procedure involving the discretization of the hollow sphere into concentric layers. Each layer has uniform secant moduli. The predictions of the model are compared with the more accurate numerical results obtained using the finite element method. Good agreement is found to exist with all the macroscopic stress triaxialities and all the porosity and nonlinearity values studied.

Keywords: Porous media, Viscoplasticity, Micro-mechanics, Double porosity

1. Introduction

The aim of this study was to develop a micromechanical model for the behavior of porous viscoplastic media containing two populations of pressurized voids.

*Corresponding author
Email addresses: jerome.julien@cea.fr (Jérôme Julien), mihai.garajeu@univ-cezanne.fr (Mihail Gărăjeu), michel@lma.cnrs-mrs.fr (Jean-Claude Michel)
[1] Present address : CEA Cadarache DEC/SESC/LSC Bât. 151, 13108 Saint-Paul lez Durance, France

The problem of modeling the behavior of viscoplastic materials containing voids is not new. Since the seminal work by Budiansky et al. (1982) on the deformation of a spherical void in an infinite block of nonlinear viscous matrix, several studies have been devoted to this subject. Duva and Hutchinson (1984) proposed an explicit form for the effective potential of nonlinear materials containing voids at dilute volume fractions and Cocks (1989) assessed this potential in a material with an arbitrary void volume fraction, based on variational principles.

More rigorous methods based on variational principles have been developed by Ponte Castañeda (1991), Willis (1991) and Michel and Suquet (1992) to obtain rigorous bounds for the effective potential of porous isotropic materials. These results are less accurate in the case of the composite-sphere assemblage subjected to purely hydrostatic loadings, and Michel and Suquet therefore proposed a correction of the bounds at high stress triaxialities (a similar correction was proposed independently by Sofronis and McMeeking (1992)), which, in the limit case of a rigid-plastic matrix, leads to the Gurson yield criterion (Gurson, 1977). Suquet (1995) has shown that these variational estimates are equivalent to the secant approach using the secant moduli of the phases evaluated at the second order moments of the fields in the phases.

Generalizing the notion of optimally selected linear comparison composite, Ponte Castañeda (1996) proposed an alternative approach whereby the tangent moduli of the phases are evaluated at the phase averages of the fields (first order moments) using a self-consistent scheme. Nebozhyn and Ponte Castañeda (1999) subsequently proposed improved estimates for nonlinear porous materials taking the effect of the third invariant of the macroscopic stress tensor into account. The latter authors also pointed out that in some cases,this method, can violate rigorous bounds or lead to nonconvex effective energy functions. In order to address this problem, Ponte Castañeda (2002) proposed a new second-order method in which the second-order moments of the local fields in the linear comparison composite are used to evaluate the tangent moduli of the phases. This new method was an improvement on the earlier method and gives more accurate estimates for the effective behavior of isotropic porous nonlinear media, but as Pastor and Ponte Castañeda (2002) noted, these estimates are too stiff at high triaxialities and nonlinearities. In a more recent study, Danas et al. (2008) used the new second-order method along with a more sophisticated choice of linear comparison composite to obtain a model for porous nonlinear materials which is consistent with nonlinear bounds, accounts for the effect of the third invariant of the macroscopic stress tensor and reproduces the behavior of the composite-sphere assemblage at high stress triaxialities (and therefore coincides with the hydrostatic limit of the Gurson's criterion in the limit case of ideal plasticity).

All these results were obtained on isotropic porous materials containing only one population of voids. However, very few studies have been devoted to modeling the behavior of porous materials containing two populations of voids of different sizes. Most of the studies on these lines have focused on the influence of the second population of voids on the behavior of ideally plastic porous materials. Perrin and Leblond (1990) gave an analytical solution to the problem of a hollow sphere consisting of a Gurson material under hydrostatic tension. Fabrègue and Pardoen (2008) carried out finite element cell simulations to determine the influence of a second population of spherical voids on the onset of the coalescence of a primary population of spheroidal voids. Vincent et al. (2009) has obtained two bounds for the behavior of porous ideally plastic materials containing two populations of pressurized voids of different sizes, which are accurate at low and high

triaxialities, respectively. These authors also proposed an estimate based on a N-phase model, inspired by Bilger et al. (2002), which matches the best of the two bounds at low and high triaxialities. In the model proposed in the present paper, the N-phase model is extended to include the case of a viscoplastic matrix.

This paper is organized as follows. Section 2 presents the class of composites under consideration, which are characterized by three separate length-scales, called the microscopic, mesoscopic and macroscopic scales. At the macroscopic scale, the composite is a porous material containing pressurized voids embedded in a compressible matrix, and at the mesoscopic scale, the matrix is a porous viscoplastic material. It is assumed that the effective properties of the matrix are those resulting from a first homogenization procedure. In the present study, the behavior of the matrix derives from a dissipation potential which is an extension of Gurson's model (Gurson, 1977) to viscous materials, proposed by Michel and Suquet (1992) (see section 2.2.2 for details). In Section 3, a semi-analytical model is proposed to account for the effective properties of the composite. The model is based on the modified secant approach proposed by Suquet (1995), and involves the use of a simplified volume element (a hollow sphere containing N concentric layers). In Section 4, the predictions of the model are compared with the numerical results of finite element calculations. The conclusions are presented in section 5.

Throughout the text, vectors and second-order tensors will be denoted with boldface letters and the various types of products will be denoted by dots (e.g., $\boldsymbol{u}.\boldsymbol{v} = u_i v_i$, $\sigma : \boldsymbol{\varepsilon} = \sigma_{ij}\varepsilon_{ij}$).

2. Problem setting

2.1. Two populations of voids of different sizes

The composites on which this study focuses are porous materials containing two populations of voids. The difference in size between the two populations of voids is large enough for the voids to be subdivided into two classes: "small" and "large" voids. To express this information in a more rigorous setting, the composite is taken to be a three-scale material showing heterogeneities at different scales, hereafter referred as the microscopic, mesoscopic and macroscopic scales. These scales are characterized by different lengths d, a and A (see Figure 1) corresponding to the size of the small voids (d), the size of the large voids (a) and the size of a very large representative volume element (A), respectively. The voids are assumed to be spherical in shape and to be isotropically arranged at the various scales.

At the mesoscopic scale the porosity is denoted f_s and represents the small void volume fraction in the domain Ω, $f_s = \frac{|S|}{|\Omega|}$, where S denotes the domain of Ω occupied by the small voids (Figure 1a). At the macroscopic scale the porosity is denoted f_l and represents the large void volume fraction in the representative volume element V, $f_l = \frac{|L|}{|V|}$, where L denotes the domain of V occupied by the large voids (Figure 1b). The total porosity of the composite is therefore:

$$f = \bar{f}_s + f_l - \bar{f}_s f_l, \tag{2.1}$$

where $\bar{f}_s$ denotes the overall small void volume fraction in the domain $V - L$. The voids are pressurized. We take p_s and p_l to denote the internal pressure in the small and large voids, respectively. The two internal pressures p_s and p_l can be different.

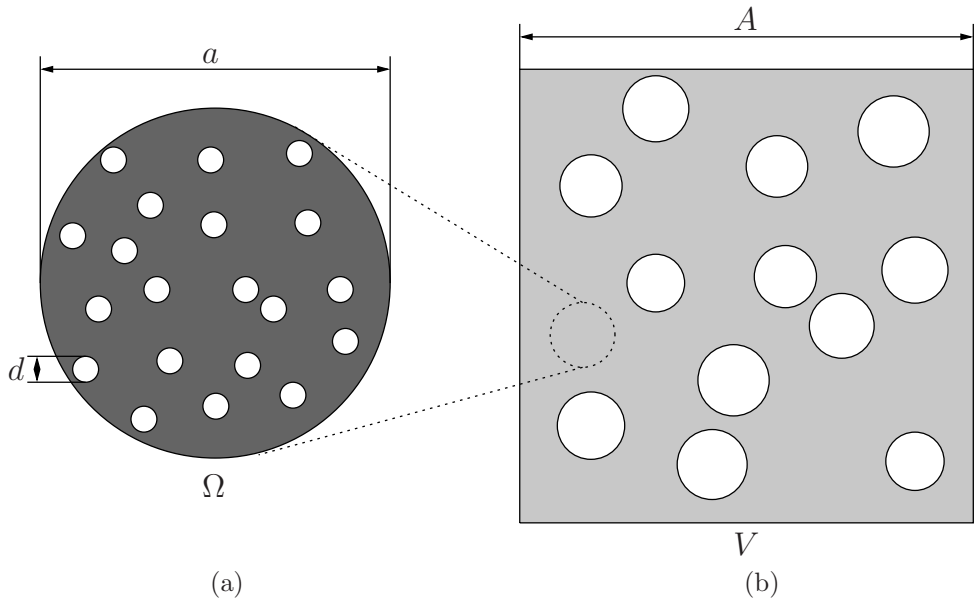

Figure 1: Two populations of voids of different sizes. (a) Representative volume element Ω at the mesoscopic scale showing the microstructure. (b) Representative volume element V at the macroscopic scale showing the mesostructure.

When the three scales are "well separated", which means that the three lengths further satisfy the string of inequalities $d \ll a \ll A$, the effective behavior of the composite can be obtained by splitting the homogenization procedure into two successive steps. Different notations are used to distinguish quantities at the three different scales. We take $\dot{\boldsymbol{e}}$, $\dot{\boldsymbol{\varepsilon}}$ and $\dot{\boldsymbol{E}}$ to denote the Eulerian strain-rate at the micoscopic, mesoscopic and macroscopic scales, respectively. Likewise, $\boldsymbol{s}$, $\boldsymbol{\sigma}$ and $\boldsymbol{\Sigma}$ denote the Cauchy stress at the three scales.

2.2. Microscopic, mesoscopic and macroscopic potentials

2.2.1. Microscopic potential

At the microscopic scale, the matrix phase is assumed to be an isotropic power-law incompressible material. Its local behavior is characterized by a *convex* dissipation potential $\varphi(\dot{\boldsymbol{e}})$ such that the microscopic strain-rate $\dot{\boldsymbol{e}}$ and the microscopic stress $\boldsymbol{s}$ are related by

$$\boldsymbol{s} = \frac{\partial \varphi}{\partial \dot{\boldsymbol{e}}}(\dot{\boldsymbol{e}}), \quad \varphi(\dot{\boldsymbol{e}}) = \frac{\sigma_0 \dot{\varepsilon}_0}{m+1} \left(\frac{\dot{e}_{eq}}{\dot{\varepsilon}_0} \right)^{m+1} \quad \text{when } \operatorname{tr}(\dot{\boldsymbol{e}}) = 0, \quad +\infty \quad \text{otherwise}, \tag{2.2}$$

where σ_0 is the flow stress, $\dot{\varepsilon}_0$ is the reference strain-rate, m is the power exponent (ranging between 0 and 1) and $\dot{e}_{eq}$ is the second isotropic invariant of $\dot{\boldsymbol{e}}$:

$$\dot{e}_{eq} = \left(\frac{2}{3} \dot{\boldsymbol{e}}^d \cdot \dot{\boldsymbol{e}}^d \right)^{\frac{1}{2}} \quad \text{with} \quad \dot{\boldsymbol{e}}^d = \dot{\boldsymbol{e}} - \dot{e}_m \boldsymbol{i} \quad \text{and} \quad \dot{e}_m = \frac{\operatorname{tr}(\dot{\boldsymbol{e}})}{3} \tag{2.3}$$

($\boldsymbol{i}$ is the second order identity tensor).

2.2.2. Examples of mesoscopic potentials in the case of small non pressurized voids

Let us first consider the case where the small voids are not pressurized ($p_s = 0$). In this case, the effective dissipation potential of the composite at the mesoscopic scale is given by the variational principle:

$$\widetilde{\varphi}(f_s, \dot{\boldsymbol{\varepsilon}}) = \inf_{\boldsymbol{v} \in \mathcal{K}(\dot{\boldsymbol{\varepsilon}})} \frac{1}{|\Omega|} \int_{\Omega - S} \varphi(\boldsymbol{e}(\boldsymbol{v})) \, \mathrm{d}\boldsymbol{x}, \tag{2.4}$$

where $\mathcal{K}(\dot{\boldsymbol{\varepsilon}})$ is the set of kinematically admissible velocity fields:

$$\mathcal{K}(\dot{\boldsymbol{\varepsilon}}) = \{\boldsymbol{v} \mid \boldsymbol{v}(\boldsymbol{x}) = \dot{\boldsymbol{\varepsilon}}.\boldsymbol{x} \text{ on } \partial\Omega, \ \operatorname{div} \boldsymbol{v}(\boldsymbol{x}) = 0 \text{ in } \Omega - S\}. \tag{2.5}$$

The dissipation potential $\widetilde{\varphi}$ is a convex function of the mesoscopic strain-rate $\dot{\boldsymbol{\varepsilon}}$. Taking the expression (2.2) for the local dissipation potential φ, (2.4) specialises to:

$$\widetilde{\varphi}(f_s, \dot{\boldsymbol{\varepsilon}}) = \frac{\sigma_0 \dot{\varepsilon}_0}{m+1} \inf_{\boldsymbol{v} \in \mathcal{K}(\dot{\boldsymbol{\varepsilon}})} \frac{1}{|\Omega|} \int_{\Omega - S} \left(\frac{e_{eq}(\boldsymbol{v})}{\dot{\varepsilon}_0} \right)^{m+1} \mathrm{d}\boldsymbol{x}. \tag{2.6}$$

The particular case $m = 1$ corresponds to a linearly viscous matrix. As it is well-known, the effective potential of linear porous materials is bounded from above by the upper Hashin-Shtrikman bound:

$$\widetilde{\varphi}(f_s, \dot{\boldsymbol{\varepsilon}}) \leq \frac{(1 - f_s)\sigma_0}{2\dot{\varepsilon}_0} \left(\frac{4}{f_s} \, \dot{\varepsilon}_m^2 + \frac{1}{1 + \frac{2}{3} f_s} \, \dot{\varepsilon}_{eq}^2 \right). \tag{2.7}$$

The other extreme case $m = 0$ corresponds to a rigid ideally plastic matrix obeying the von Mises criterion with flow stress σ_0. The most widely used model for ideally plastic porous materials is due to Gurson (1977) and it is based on the approximate analysis of a single hollow sphere. The Gurson yield function takes the form:

$$\frac{\sigma_{eq}^2}{\sigma_0} + 2 f_s \cosh\left(\frac{3}{2} \frac{\sigma_m}{\sigma_0} \right) - 1 - f_s^2 \leq 0, \tag{2.8}$$

where σ_m and σ_{eq} are the usual mean and von Mises equivalent stresses, respectively. It can be shown (see for instance Gărăjeu et al. (2000)) that the dissipation potential $\widetilde{\varphi}$, associated with the Gurson yield function, reads as follows:

$$\widetilde{\varphi}(f_s, \dot{\boldsymbol{\varepsilon}}) = \sigma_0 \int_{f_s}^{1} \left(\frac{4\dot{\varepsilon}_m^2}{y^2} + \dot{\varepsilon}_{eq}^2 \right)^{1/2} \mathrm{d}y. \tag{2.9}$$

With intermediate values of m, Leblond et al. (1994) and Gărăjeu et al. (2000), generalizing the analysis of Gurson with the same velocity fields, have proposed a dissipation potential which reads:

$$\widetilde{\varphi}(f_s, \dot{\boldsymbol{\varepsilon}}) = \frac{1}{m+1} \frac{\sigma_0}{\dot{\varepsilon}_0^m} \int_{f_s}^{1} \left(\frac{4\dot{\varepsilon}_m^2}{y^2} + \dot{\varepsilon}_{eq}^2 \right)^{\frac{m+1}{2}} \mathrm{d}y. \tag{2.10}$$

When $m = 0$, this dissipation potential (2.10) reduces to that of Gurson (2.9). When $m = 1$, it coincides with the upper Hashin-Shtrikman bound (2.7) for hydrostatic loadings but slightly exceeds this bound in the case of deviatoric loadings. Nonlinear bounds for power-law or ideally-plastic porous materials have been obtained using variational methods (Ponte Castañeda (1991, 1992), Willis (1991), Suquet (1992, 1993)). Although they are rigorous upper bounds, these nonlinear bounds improve the Gurson criterion at low stress triaxialities but are known to be inaccurate at high stress triaxialities. Michel and Suquet (1992) have proposed a simple estimate of the form:

$$\widetilde{\varphi}(f_s, \dot{\boldsymbol{\varepsilon}}) = \frac{\sigma_0 \dot{\varepsilon}_0}{m+1} \left[\frac{4}{A(f_s,m)} \left(\frac{\dot{\varepsilon}_m}{\dot{\varepsilon}_0} \right)^2 + \frac{1}{B(f_s,m)} \left(\frac{\dot{\varepsilon}_{eq}}{\dot{\varepsilon}_0} \right)^2 \right]^{\frac{m+1}{2}}, \tag{2.11}$$

with

$$A(f_s,m) = \left(\frac{f_s^{-m} - 1}{m} \right)^{\frac{-2}{m+1}}, \quad B(f_s,m) = \left(1 + \frac{2}{3} f_s \right) (1 - f_s)^{\frac{-2}{m+1}}. \tag{2.12}$$

This estimate satisfies the bounds and reproduces the exact solution of the hollow sphere consisting of a power-law viscous matrix under hydrostatic loading conditions (a similar correction was proposed independently by Sofronis and McMeeking (1992)).

A more general model depending on the third invariant of the stress, based on the second-order method by Ponte Castañeda (2002),was recently proposed by Danas et al. (2008). Exact results on a special class of nonlinear porous materials with sequentially laminated microstructures were obtained by Idiart (2008).

2.2.3. From small non pressurized to pressurized voids

Let us now take the case where small voids are subjected to an internal pressure p_s. The definition (2.4) needs to be changed in this case. The variational principle giving the effective dissipation potential at the mesoscopic scale now reads:

$$\phi(f_s, \dot{\boldsymbol{\varepsilon}}, p_s) = \inf_{\boldsymbol{v} \in \mathcal{K}(\dot{\boldsymbol{\varepsilon}})} \frac{1}{|\Omega|} \left[\int_{\Omega - S} \varphi(\boldsymbol{e}(\boldsymbol{v}))\, \mathrm{d}\boldsymbol{x} + p_s \int_{\partial S} \boldsymbol{v} \cdot \boldsymbol{n}\, \mathrm{d}s \right], \tag{2.13}$$

where $\boldsymbol{n}$ is the outer normal to ∂S (*i.e.*, the normal pointing towards the interior of the small voids).

Using Lemma 1 (its proof is given in the Appendix Appendix B):

Lemma 1. *For any field $\boldsymbol{v} \in \mathcal{K}(\dot{\boldsymbol{\varepsilon}})$, the following holds:*

$$\frac{1}{|\Omega|} \int_{\partial S} \boldsymbol{v} \cdot \boldsymbol{n}\, \mathrm{d}s = \frac{1}{|\Omega|} \int_{\Omega - S} \operatorname{div} \boldsymbol{v}\, \mathrm{d}\boldsymbol{x} - \operatorname{tr}(\dot{\boldsymbol{\varepsilon}}), \tag{2.14}$$

it follows that since the matrix is incompressible ($\operatorname{div} \boldsymbol{v} = 0$ in $\Omega - S$), the last term of (2.13) can be reduced to

$$\frac{1}{|\Omega|} \int_{\partial S} \boldsymbol{v} \cdot \boldsymbol{n}\, \mathrm{d}s = -\operatorname{tr}(\dot{\boldsymbol{\varepsilon}}).$$

The mesoscopic effective dissipation potential therefore reads:

$$\begin{aligned}\phi(f_s,\dot{\boldsymbol{\varepsilon}},p_s) &= \inf_{\boldsymbol{v}\,\in\,\mathcal{K}(\dot{\boldsymbol{\varepsilon}})}\left[\frac{1}{|\Omega|}\int_{\Omega-S}\varphi(\boldsymbol{e}(\boldsymbol{v}))\,\mathrm{d}\boldsymbol{x}\right]-p_s\,\mathrm{tr}\,(\dot{\boldsymbol{\varepsilon}})\,,\\ &= \widetilde{\varphi}(f_s,\dot{\boldsymbol{\varepsilon}})-p_s\,\mathrm{tr}\,(\dot{\boldsymbol{\varepsilon}})\,. \end{aligned}\tag{2.15}$$

Equation (2.15) shows that in the case of an incompressible matrix, the effective dissipation potential of the satured porous medium (voids having a non-zero internal pressure p_s) can be simply deduced from that obtained in the case when the voids are not pressurized by the relation:

$$\phi(f_s,\dot{\boldsymbol{\varepsilon}},p_s)=\widetilde{\varphi}(f_s,\dot{\boldsymbol{\varepsilon}})-3p_s\dot{\varepsilon}_m.\tag{2.16}$$

2.2.4. Macroscopic potential

Knowing the microstructure of the representative volume element V and the pressure p_l in the large voids, and assuming that the mesoscopic effective dissipation potential $\phi(f_s,\dot{\boldsymbol{\varepsilon}},p_s)$ is known, the question is now to determine the macroscopic effective dissipation potential Φ of the composite.

The definition of Φ is similar to that of the mesoscopic potential (2.13) :

$$\Phi(\dot{\boldsymbol{E}})^2=\inf_{\boldsymbol{v}\,\in\,\overline{\mathcal{K}}(\dot{\boldsymbol{E}})}\frac{1}{|V|}\left[\int_{V-L}\phi(f_s,\boldsymbol{\varepsilon}(\boldsymbol{v}),p_s)\,\mathrm{d}\boldsymbol{x}+p_l\int_{\partial L}\boldsymbol{v}\cdot\boldsymbol{n}\,\mathrm{d}s\right],\tag{2.17}$$

where, since the porous matrix is compressible at the mesoscopic scale, the set of kinematically admissible velocity fields is now defined by:

$$\overline{\mathcal{K}}(\dot{\boldsymbol{E}})=\left\{\boldsymbol{v}\mid\boldsymbol{v}(\boldsymbol{x})=\dot{\boldsymbol{E}}.\boldsymbol{x}\text{ on }\partial V\right\}.\tag{2.18}$$

Due to the compressibility of the porous matrix at the mesoscopic scale, the translation rule (2.16) cannot be applied to the macroscopic dissipation potential Φ. However, using (2.16), the variational principle (2.17) can be written in the following form:

$$\Phi(\dot{\boldsymbol{E}})=\inf_{\boldsymbol{v}\,\in\,\overline{\mathcal{K}}(\dot{\boldsymbol{E}})}\frac{1}{|V|}\left[\int_{V-L}\widetilde{\varphi}(f_s,\boldsymbol{\varepsilon}(\boldsymbol{v}))\,\mathrm{d}\boldsymbol{x}-p_s\int_{V-L}\mathrm{tr}\,(\boldsymbol{\varepsilon}(\boldsymbol{v}))\;\mathrm{d}\boldsymbol{x}+p_l\int_{\partial L}\boldsymbol{v}\cdot\boldsymbol{n}\,\mathrm{d}s\right].\tag{2.19}$$

¿From Lemma 1, it follows:

$$\frac{1}{|V|}\int_{V-L}\mathrm{tr}\,(\boldsymbol{\varepsilon}(\boldsymbol{v}))\;\mathrm{d}\boldsymbol{x}=\frac{1}{|V|}\int_{V-L}\mathrm{div}\,\boldsymbol{v}\,\mathrm{d}\boldsymbol{x}=\frac{1}{|V|}\int_{\partial L}\boldsymbol{v}\cdot\boldsymbol{n}\,\mathrm{d}s+\mathrm{tr}\left(\dot{\boldsymbol{E}}\right).$$

The macroscopic effective dissipation potential is then given by:

$$\Phi(\dot{\boldsymbol{E}})=\inf_{\boldsymbol{v}\,\in\,\overline{\mathcal{K}}(\dot{\boldsymbol{E}})}\frac{1}{|V|}\left[\int_{V-L}\widetilde{\varphi}(f_s,\boldsymbol{\varepsilon}(\boldsymbol{v}))\,\mathrm{d}\boldsymbol{x}+(p_l-p_s)\int_{\partial L}\boldsymbol{v}\cdot\boldsymbol{n}\,\mathrm{d}s\right]-3p_s\dot{E}_m.\tag{2.20}$$

[2]To simplify the notation, the dependence of Φ on f_s, f_l, p_s and p_l is omitted.

Equation (2.20) reveals the quantity

$$\widetilde{\Phi}(f_s, f_l, \dot{\boldsymbol{E}}, p) = \inf_{\boldsymbol{v} \in \overline{\mathcal{K}}(\dot{\boldsymbol{E}})} \frac{1}{|V|} \left[\int_{V-L} \widetilde{\varphi}(f_s, \boldsymbol{\varepsilon}(\boldsymbol{v}))\, \mathrm{d}\boldsymbol{x} + p \int_{\partial L} \boldsymbol{v} \cdot \boldsymbol{n}\, \mathrm{d}s \right], \tag{2.21}$$

that is, the macroscopic effective dissipation potential of a composite with the same microstructure, but where the small voids are stress-free and the large voids are subjected to the difference of pressure $p = p_l - p_s$.

Remark. Equation (2.20) (see also Vincent et al. (2009) for a similar previous result) shows that any estimate or bound for the effective dissipation potential $\widetilde{\Phi}$ will yield a corresponding estimate or bound for the effective dissipation potential Φ. Therefore, in what follows, only the simpler case where the small voids are not pressurized can be considered.

To find the velocity field $\dot{\boldsymbol{u}}$ that realizes the infimum in (2.21), the following local problem must be solved:

$$\begin{cases} \boldsymbol{\sigma} = \dfrac{\partial \widetilde{\varphi}}{\partial \dot{\boldsymbol{\varepsilon}}}(f_s, \boldsymbol{\varepsilon}(\dot{\boldsymbol{u}})) \quad \text{in } V - L, \\ \operatorname{div} \boldsymbol{\sigma} = 0 \quad \text{in } V - L, \\ \boldsymbol{\sigma}.\boldsymbol{n} = -p\, \boldsymbol{n} \quad \text{on } \partial L, \\ \dot{\boldsymbol{u}} = \dot{\boldsymbol{E}}.\boldsymbol{x} \quad \text{on } \partial V. \end{cases} \tag{2.22}$$

The next section presents a semi-analytical approach to estimate the velocity field $\dot{\boldsymbol{u}}$ (and therefore the effective dissipation potential (2.21)) solution of (2.22).

3. Semi-analytical model

3.1. First step: a secant approach

In order to estimate the local velocity field solution of the nonlinear problem (2.22), a secant linearization approach is used. The behavior of the porous matrix derives from a dissipation potential $\widetilde{\varphi}$ which is assumed to depend on the strain-rate through its first two isotropic invariants, $\widetilde{\varphi}(\dot{\boldsymbol{\varepsilon}}) = \widetilde{\varphi}(\dot{\varepsilon}_m, \dot{\varepsilon}_{eq})$. The local behavior is then given by:

$$\boldsymbol{\sigma} = \frac{1}{3} \frac{\partial \widetilde{\varphi}}{\partial \dot{\varepsilon}_m}\, \boldsymbol{i} + \frac{2}{3} \frac{\partial \widetilde{\varphi}}{\partial \dot{\varepsilon}_{eq}}\, \frac{\dot{\boldsymbol{\varepsilon}}^d}{\dot{\varepsilon}_{eq}}. \tag{3.23}$$

Relation (3.23) looks like a linear stress - strain-rate relation:

$$\boldsymbol{\sigma} = 3k\, \dot{\varepsilon}_m\, \boldsymbol{i} + 2\mu\, \dot{\boldsymbol{\varepsilon}}^d, \tag{3.24}$$

with secant moduli k and μ depending on the local strain-rate:

$$k = \frac{1}{9\dot{\varepsilon}_m} \frac{\partial \widetilde{\varphi}}{\partial \dot{\varepsilon}_m}(\dot{\varepsilon}_m, \dot{\varepsilon}_{eq}), \quad \mu = \frac{1}{3\dot{\varepsilon}_{eq}} \frac{\partial \widetilde{\varphi}}{\partial \dot{\varepsilon}_{eq}}(\dot{\varepsilon}_m, \dot{\varepsilon}_{eq}). \tag{3.25}$$

The porous matrix can therefore be regarded as a composite containing an infinitely large number of linear phases with material coefficients depending on the local strain-rate field. To the best of our knowledge, this nonlinear problem has no analytical solution.

An approximation of this problem can be obtained by assuming that the porous matrix contains only N linear phases with uniform moduli k_i and μ_i, $i = 1, 2, ..., N$, which still depend on the local strain-rate, but in the following way:

$$k_i = \frac{1}{9\dot{\epsilon}_m^{(i)}} \frac{\partial \widetilde{\varphi}}{\partial \dot{\varepsilon}_m}(\dot{\epsilon}_m^{(i)}, \dot{\epsilon}_{eq}^{(i)}), \quad \mu_i = \frac{1}{3\dot{\epsilon}_{eq}^{(i)}} \frac{\partial \widetilde{\varphi}}{\partial \dot{\varepsilon}_{eq}}(\dot{\epsilon}_m^{(i)}, \dot{\epsilon}_{eq}^{(i)}). \tag{3.26}$$

In the classical secant method, $\dot{\epsilon}_m^{(i)}$ and $\dot{\epsilon}_{eq}^{(i)}$ are taken to be the average over the phase i of $\dot{\varepsilon}_m$ and $\dot{\varepsilon}_{eq}$, respectively, $\dot{\epsilon}_m^{(i)} = \langle \dot{\varepsilon}_m \rangle_i$, $\dot{\epsilon}_{eq}^{(i)} = \langle \dot{\varepsilon}_{eq} \rangle_i$ ($\langle \cdot \rangle_i$ is the average operator over the phase i). In the present model, use is made of the modified secant method proposed by Suquet (1995) which is equivalent to the variational method by Ponte Castañeda (1992). The secant moduli (3.26) are evaluated using the second-order moments of the strain-rate field:

$$\dot{\epsilon}_m^{(i)} = \left\langle \dot{\varepsilon}_m^2 \right\rangle_i^{\frac{1}{2}}, \quad \dot{\epsilon}_{eq}^{(i)} = \left\langle \dot{\varepsilon}_{eq}^2 \right\rangle_i^{\frac{1}{2}}. \tag{3.27}$$

The secant approach makes it possible to transform the initial local problem (2.22) into a new local problem involving a composite consisting of N linear phases. Let $V^{(i)}$ denote the domain occupied by the phase i, $V - L = \cup_{i=1}^{N} V^{(i)}$. Then the equations for the linearized problem are:

$$\begin{cases} \boldsymbol{\sigma} = 3k_i\, \dot{\varepsilon}_m\, \boldsymbol{i} + 2\mu_i\, \dot{\boldsymbol{\varepsilon}}^d & \text{in } V^{(i)}, \\ \operatorname{div} \boldsymbol{\sigma} = 0 & \text{in } V - L, \\ \boldsymbol{\sigma}.\boldsymbol{n} = -p\, \boldsymbol{n} & \text{on } \partial L, \\ \dot{\boldsymbol{u}}(\boldsymbol{x}) = \dot{\boldsymbol{E}}.\boldsymbol{x} & \text{on } \partial V, \end{cases} \tag{3.28}$$

where the secant moduli k_i and μ_i are given by (3.26-3.27).

Given a prescribed macroscopic strain-rate $\dot{\boldsymbol{E}}$, the solution of this problem is obtained by a fixed-point procedure:

Iterate r: Being known the values of the secant moduli $k_i^{(r-1)}$ and $\mu_i^{(r-1)}$ in all the phases ($i = 1, .., N$) at the iterate $r - 1$:

Step 1: Solve the linear problem (3.28) with $k_i = k_i^{(r-1)}$ and $\mu_i = \mu_i^{(r-1)}$ in $V^{(i)}$, $i = 1, .., N$.

Step 2: Use the local strain-rate field $\dot{\boldsymbol{\varepsilon}}$ solution obtained at step 1 to update the new secant moduli $k_i^{(r)}$ and $\mu_i^{(r)}$ given by (3.26-3.27), $i = 1, .., N$.

End: The procedure is stopped when the difference between secant moduli is small, $\left| k_i^{(r)} - k_i^{(r-1)} \right| \leq \delta \left| k_i^{(r)} \right|$, $\left| \mu_i^{(r)} - \mu_i^{(r-1)} \right| \leq \delta \left| \mu_i^{(r)} \right|$, $\delta = 10^{-6}$, $i = 1, .., N$.

This approach generally requires the use of a numerical method (like the finite element method) at each iterate r in order to solve the linear problem (step 1) and a numerical integration to calculate the averages over each phase i (step 2). The behavior of the representative volume element V obtained using this approach is then applied in a structure computation, which may need thousands of calls of this procedure. In order to minimize the computation time, it is worth having analytical results on the macroscopic behavior of the representative volume element V. The next section presents one possible way of reaching this goal.

3.2. Step two: a simplified volume element

In order to obtain an analytical solution to the linear problem, we consider a representative volume element V consisting of a hollow sphere with the internal radius a and the external radius b. The central cavity L (radius $r_0 = a$) is pressurized (pressure p) and the matrix is formed of N concentric layers ($r_N = b$), all of which show linear behavior and secant moduli k_i and μ_i, $i = 1, .., N$ (Figure 2).

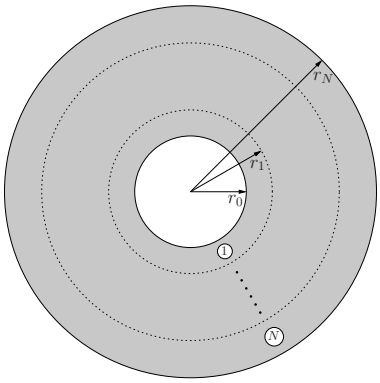

Figure 2: Simplified volume element: a hollow sphere containing N concentric layers.

A similar approach has been proposed by Hervé and Zaoui (1993) in the case of linear materials containing rigid inclusions and by Bilger et al. (2002) in that of ideally plastic porous materials. Unlike the approach presented here, the authors of these two studies are interested in obtaining a self-consistent estimate, and the simplified volume element is therefore embedded in an infinitely large equivalent matrix.

In line with Hervé and Zaoui (1993), since the behavior of the layers is linear, the velocity field solution of the linear problem (3.28) can be decomposed into the sum of three velocity fields

$$\dot{\boldsymbol{u}} = \dot{\boldsymbol{u}}_1 + \dot{\boldsymbol{u}}_2 + \dot{\boldsymbol{u}}_3, \tag{3.29}$$

corresponding to the following boundary conditions, respectively:

$$\left\{ \begin{array}{l} \boldsymbol{\sigma}.\boldsymbol{n} = -p\boldsymbol{n} \text{ on } \partial L \\ \dot{\boldsymbol{u}}_1(\boldsymbol{x}) = \dot{E}_m \boldsymbol{x} \text{ on } \partial V \end{array} \right. , \quad \left\{ \begin{array}{l} \boldsymbol{\sigma}.\boldsymbol{n} = 0 \text{ on } \partial L \\ \dot{\boldsymbol{u}}_2(\boldsymbol{x}) = \dot{\beta}\boldsymbol{\Delta}_{12}\boldsymbol{x} \text{ on } \partial V \end{array} \right. , \quad \left\{ \begin{array}{l} \boldsymbol{\sigma}.\boldsymbol{n} = 0 \text{ on } \partial L \\ \dot{\boldsymbol{u}}_3(\boldsymbol{x}) = \dot{\gamma}\boldsymbol{\Delta}_{13}\boldsymbol{x} \text{ on } \partial V. \end{array} \right. \tag{3.30}$$

In (3.30), $\boldsymbol{\Delta}_{12}$ and $\boldsymbol{\Delta}_{13}$ are deviatoric tensors:

$$\boldsymbol{\Delta}_{12} = \boldsymbol{e}_1 \otimes \boldsymbol{e}_1 - \boldsymbol{e}_2 \otimes \boldsymbol{e}_2, \quad \boldsymbol{\Delta}_{13} = \boldsymbol{e}_1 \otimes \boldsymbol{e}_1 - \boldsymbol{e}_3 \otimes \boldsymbol{e}_3, \tag{3.31}$$

where ($\boldsymbol{e}_1$, $\boldsymbol{e}_2$, $\boldsymbol{e}_3$) is the principal basis of the macroscopic strain-rate $\dot{\boldsymbol{E}}$, and $\dot{\beta}\,\boldsymbol{\Delta}_{12} + \dot{\gamma}\,\boldsymbol{\Delta}_{13} = \dot{\boldsymbol{E}}^d$ ($\dot{\boldsymbol{E}}^d$ is the deviatoric part of $\dot{\boldsymbol{E}}$).

In the basis ($\boldsymbol{e}_r$, $\boldsymbol{e}_\theta$, $\boldsymbol{e}_\varphi$) of spherical coordinates (r, θ, φ), following Christensen (1991) and Hervé and Zaoui (1993), the solutions to these three problems in each layer

i, $i = 1, .., N$, take the form:

$$\dot{\boldsymbol{u}}_1^{(i)} = \dot{u}^{(i)}(r)\boldsymbol{e}_r, \qquad \dot{u}^{(i)}(r) = F_i\, r + \frac{G_i}{r^2} \tag{3.32}$$

$$\dot{\boldsymbol{u}}_2^{(i)} = \dot{u}_r^{(i)}\boldsymbol{e}_r + \dot{u}_\theta^{(i)}\boldsymbol{e}_\theta + \dot{u}_\varphi^{(i)}\boldsymbol{e}_\varphi, \qquad \left\{ \begin{array}{l} \dot{u}_r^{(i)} = \dot{\beta}\, U^{(i)}(r) \sin^2\theta \cos 2\varphi \\ \dot{u}_\theta^{(i)} = \dot{\beta}\, V^{(i)}(r) \sin\theta \cos\theta \cos 2\varphi \\ \dot{u}_\varphi^{(i)} = -\dot{\beta}\, V^{(i)}(r) \sin\theta \sin 2\varphi \end{array} \right. \tag{3.33}$$

$$\dot{\boldsymbol{u}}_3^{(i)} = \dot{v}_r^{(i)}\boldsymbol{e}_r + \dot{v}_\theta^{(i)}\boldsymbol{e}_\theta + \dot{v}_\varphi^{(i)}\boldsymbol{e}_\varphi, \qquad \left\{ \begin{array}{l} \dot{v}_r^{(i)} = \dot{\gamma}\, U^{(i)}(r) \left(\cos^2\varphi \sin^2\theta - \cos^2\theta\right) \\ \dot{v}_\theta^{(i)} = \dot{\gamma}\, V^{(i)}(r) \left(\cos^2\varphi + 1\right) \sin\theta \cos\theta \\ \dot{v}_\varphi^{(i)} = -\dot{\gamma}\, V^{(i)}(r) \sin\varphi \cos\varphi \sin\theta \end{array} \right. \tag{3.34}$$

with

$$\left\{ \begin{array}{l} U^{(i)}(r) = A_i r - 6\dfrac{\nu_i}{1-2\nu_i} B_i r^3 + 3\dfrac{C_i}{r^4} + \dfrac{5-4\nu_i}{1-2\nu_i}\dfrac{D_i}{r^2}, \\ \\ V^{(i)}(r) = A_i r - \dfrac{7-4\nu_i}{1-2\nu_i} B_i r^3 - 2\dfrac{C_i}{r^4} + 2\dfrac{D_i}{r^2}. \end{array} \right. \tag{3.35}$$

Coefficients A_i, B_i, C_i, D_i, F_i and G_i ($i = 1, .., N$) are obtained by solving two independent linear systems: one to obtain coefficients F_i and G_i and the other to obtain A_i, B_i, C_i and D_i. As usual, the equations for these two systems express the continuity of the velocity field and the stress vector at the interfaces between layers and the corresponding boundary conditions (see Appendix Appendix A for more details)

The solution of these two systems cannot be obtained analytically even in the case of a small number of layers. However, as discussed in section 4, only a few layers (10 to 20 layers) are required to be able to obtain a good approximate solution of the nonlinear problem (2.22).

It is worth noting that the secant moduli (3.26-3.27) can be obtained analytically (no numerical integration is required): straightforward although rather complex calculations[3] give the following expressions for the second-order moments:

$$\left\langle \dot{\varepsilon}_m^2 \right\rangle_i = F_i^2 + \frac{4}{5}(\dot{\beta}^2 + \dot{\beta}\dot{\gamma} + \dot{\gamma}^2)\, [B_i,\, D_i]\, P_m^{(i)} \left[\begin{array}{c} B_i \\ D_i \end{array} \right], \tag{3.36}$$

$$\left\langle \dot{\varepsilon}_{eq}^2 \right\rangle_i = \frac{4G_i^2}{r_i^3\, r_{i-1}^3} + \frac{4}{5}(\dot{\beta}^2 + \dot{\beta}\dot{\gamma} + \dot{\gamma}^2) \left[A_i,\, \frac{B_i}{1-2\nu_i},\, C_i,\, \frac{D_i}{1-2\nu_i} \right] P_{eq}^{(i)} \left[\begin{array}{c} A_i \\ \frac{B_i}{1-2\nu_i} \\ C_i \\ \frac{D_i}{1-2\nu_i} \end{array} \right] \tag{3.37}$$

where $P_m^{(i)}$ and $P_{eq}^{(i)}$ are the two following matrices:

$$P_m^{(i)} = \left[\begin{array}{cc} \frac{7\left(r_i^7 - r_{i-1}^7\right)}{r_i^3 - r_{i-1}^3} & -\frac{7\left(r_i^2 - r_{i-1}^2\right)}{r_i^3 - r_{i-1}^3} \\ -\frac{7\left(r_i^2 - r_{i-1}^2\right)}{r_i^3 - r_{i-1}^3} & \frac{4}{3 r_{i-1}^3 r_i^3} \end{array} \right], \tag{3.38}$$

[3] Mathematica has been used to perform these calculations.

and

$$P_{eq}^{(i)} = \begin{bmatrix} \frac{5}{3} & -\frac{7\left(r_i^5-r_{i-1}^5\right)}{r_i^3-r_{i-1}^3} & 0 & 0 \\ -\frac{7\left(r_i^5-r_{i-1}^5\right)}{r_i^3-r_{i-1}^3} & \frac{\left(r_i^7-r_{i-1}^7\right)\left(8\nu_i^2+35\right)}{r_i^3-r_{i-1}^3} & 0 & \frac{4\left(r_i^2-r_{i-1}^2\right)(5-7\nu_i)\nu_i}{r_i^3-r_{i-1}^3} \\ 0 & 0 & \frac{40\left(r_i^7-r_{i-1}^7\right)}{r_{i-1}^7 r_i^7\left(r_i^3-r_{i-1}^3\right)} & \frac{24\left(r_i^5-r_{i-1}^5\right)}{r_{i-1}^5 r_i^5\left(r_i^3-r_{i-1}^3\right)} \\ 0 & \frac{4\left(r_i^2-r_{i-1}^2\right)(5-7\nu_i)\nu_i}{r_i^3-r_{i-1}^3} & \frac{24\left(r_i^5-r_{i-1}^5\right)}{r_{i-1}^5 r_i^5\left(r_i^3-r_{i-1}^3\right)} & \frac{8\left(7\nu_i^2-10\nu_i+10\right)}{3r_{i-1}^3 r_i^3} \end{bmatrix}. \tag{3.39}$$

Note also that the matrix $P_m^{(i)}$ depends on the geometry of the layer i, whereas it is independent of the secant moduli k_i and μ_i. Therefore, in the fixed-point procedure described at the beginning of this section, it remains unchanged. Unlike $P_m^{(i)}$, the matrix $P_{eq}^{(i)}$ generally changes from one step to another, since it depends on the coefficient ν_i. However, in the case where the mesoscopic dissipation potential is of the form (2.11), all the layers have the same secant Poisson coefficient $\nu = \frac{2B-A}{4B+A}$ (A and B are the coefficients (2.12)), which is independent of the second moments of the strain-rate. In this case, $P_{eq}^{(i)}$ also remains unchanged in the fixed-point procedure.

4. Validation of the model

In the previous section, a constitutive model for isotropic viscoplastic porous materials containing two populations of pressurized voids of different sizes was presented. The model is based on a secant linearization procedure of the behavior of the porous matrix coupled with analytical results obtained on a simplified volume element. The aim of the present section is to assess the accuracy of this semi-analytical approach by comparing the predictions obtained with the results of full-field finite element calculations.

4.1. Validation procedure

The effective behavior of porous viscoplastic materials is commonly represented in terms of equipotential surfaces of the stress potential Ψ, dual of Φ. As discussed above in section 2.2.4, when both populations of voids are pressurized, the macroscopic dissipation potential Φ (and therefore its dual Ψ) can be deduced from that obtained taking the small voids to be stress-free and the large voids to be subjected to the difference of pressure $p = p_l - p_s$. It therefore suffices to validate the model in the case where $p_s = 0$ and $p_l \neq 0$. The following equipotential surface is considered[1]:

$$\widetilde{\Psi}(\boldsymbol{\Sigma}, p_l) = \frac{\sigma_0 \dot{\varepsilon}_0}{n+1}, \quad \widetilde{\Psi}(\boldsymbol{\Sigma}, p_l) = \inf_{\boldsymbol{\tau} \in \mathcal{S}(\boldsymbol{\Sigma}, p_l)} \frac{1}{|V|} \int_{V-L} \widetilde{\psi}(f_s, \boldsymbol{\tau}) \, \mathrm{d}\boldsymbol{x}, \tag{4.40}$$

where $\mathcal{S}(\boldsymbol{\Sigma}, p_l)$ denotes the set of statically admissible stress fields with the macroscopic stress $\boldsymbol{\Sigma}$ and the internal pressure p_l in the large voids,

$$\begin{aligned} \mathcal{S}(\boldsymbol{\Sigma}, p_l) = \{ &\boldsymbol{\tau} / \ \mathrm{div}\,(\boldsymbol{\tau}) = 0 \text{ in } V - L, \\ &\boldsymbol{\tau}.\boldsymbol{n} = -p_l \, \boldsymbol{n} \text{ on } \partial L, \quad \tfrac{1}{|V|} \textstyle\int_{\partial V} \boldsymbol{\tau}.\boldsymbol{n} \otimes_s \boldsymbol{x} \, \mathrm{d}s = \boldsymbol{\Sigma} \}, \end{aligned} \tag{4.41}$$

[1] To simplify the notation, the dependence of $\widetilde{\Psi}$ on f_s and f_l is omitted.

$\widetilde{\psi}$ is the stress potential of the porous matrix, and $n = 1/m$. All the simulations were performed using for $\widetilde{\psi}$ the dual potential of (2.11), *i.e.*,

$$\widetilde{\psi}(f_s, \boldsymbol{\sigma}) = \frac{\sigma_0 \dot{\varepsilon}_0}{n+1} \left[\frac{9}{4} A(f_s, \frac{1}{n}) \left(\frac{\sigma_m}{\sigma_0} \right)^2 + B(f_s, \frac{1}{n}) \left(\frac{\sigma_{eq}}{\sigma_0} \right)^2 \right]^{\frac{n+1}{2}}, \tag{4.42}$$

where A and B are the coefficients given by (2.12). From the positive homogeneity of $\widetilde{\psi}$ in $\boldsymbol{\sigma}$, and given the definition $(4.40)_2$ with (4.41) of the macroscopic stress potential $\widetilde{\Psi}$, it is worth noting that $\widetilde{\Psi}$ is positively homogeneous of degree $n+1$ in $\boldsymbol{\Sigma}$ and p_l, *i.e.*, it satisfies $\widetilde{\Psi}(\lambda \boldsymbol{\Sigma}, \lambda p_l) = |\lambda|^{n+1} \widetilde{\Psi}(\boldsymbol{\Sigma}, p_l)$ for all λ.

The principle of construction of the equipotential surface $(4.40)_1$ is the following. Being prescribed a macroscopic stress direction $\boldsymbol{\Sigma}^0$ and an internal pressure p_l in the large voids, we seek the stress level λ such that:

$$\widetilde{\Psi}(\lambda \boldsymbol{\Sigma}^0, p_l) = \frac{\sigma_0 \dot{\varepsilon}_0}{n+1}. \tag{4.43}$$

The procedure is repeated in various macroscopic stress directions $\boldsymbol{\Sigma}^0$. Two cases have to be distinguished, depending on whether $p_l = 0$ or $p_l \neq 0$.

Case $p_l = 0$.. In this case, it follows from the positive homogeneity property of degree $n+1$ of the macroscopic stress potential $\widetilde{\Psi}$ that:

$$\lambda = \left[\frac{\sigma_0 \dot{\varepsilon}_0}{(n+1) \widetilde{\Psi}(\boldsymbol{\Sigma}^0, 0)} \right]^{\frac{1}{n+1}}. \tag{4.44}$$

The stress level λ is thus determined once $\widetilde{\Psi}(\boldsymbol{\Sigma}^0, 0)$ is known. In addition, taking $\dot{\boldsymbol{E}}^0$ to denote the macroscopic strain-rate associated with $\boldsymbol{\Sigma}^0$, the macroscopic strain-rate $\dot{\boldsymbol{E}}$ corresponding to the macroscopic stress $\boldsymbol{\Sigma} = \lambda \boldsymbol{\Sigma}^0$, laying on the equipotential surface, is given by:

$$\dot{\boldsymbol{E}} = \lambda^n \dot{\boldsymbol{E}}^0, \quad \dot{\boldsymbol{E}}^0 = \frac{\partial \widetilde{\Psi}}{\partial \boldsymbol{\Sigma}} (\boldsymbol{\Sigma}^0, 0). \tag{4.45}$$

Case $p_l \neq 0$.. In this case, since the porous matrix is compressible, the stress level λ which satisfies (4.43) can no longer be obtained analytically and it is necessary to proceed by performing successive iterations. When $p_l \neq 0$, the stress level λ and the corresponding macroscopic strain-rate $\dot{\boldsymbol{E}}$ are obtained numerically using a bisection method on λ.

In both cases ($p_l = 0$ or $p_l \neq 0$), for a given macroscopic stress $\boldsymbol{\Sigma}^i$ ($i = 0$ when $p_l = 0$ and $\boldsymbol{\Sigma}^i = \lambda^i \boldsymbol{\Sigma}^0$, where i is the index of iterations, when $p_l \neq 0$), the aim is to calculate the value of the macroscopic stress potential at this point, *i.e.*, $\widetilde{\Psi}(\boldsymbol{\Sigma}^i, p_l)$.

The problem to be solved in order to obtain the value of $\widetilde{\Psi}(\boldsymbol{\Sigma}^i, p_l)$ is slightly different from that considered in (2.22) and (3.28): in the present case, it is a macroscopic stress which is prescribed and not the macroscopic strain-rate $\dot{\boldsymbol{E}}$. The macroscopic strain-rate becomes an unknown in the problem and the corresponding equation for determining its

value is the condition that the average stress should be equal to the macroscopic stress. The fourth equation in (2.22) and (3.28) is replaced by:

$$\begin{aligned} &\dot{\boldsymbol{u}} = \dot{\boldsymbol{E}}^i.\boldsymbol{x} \quad \text{on } \partial V, \quad \dot{\boldsymbol{E}}^i \text{ unknown}, \\ &\frac{1}{|V|}\int_{\partial V} \boldsymbol{\sigma}.\boldsymbol{n} \otimes_s \boldsymbol{x}\, \mathrm{d}s = \boldsymbol{\Sigma}^i, \quad \boldsymbol{\Sigma}^i \text{ given}. \end{aligned} \tag{4.46}$$

The changes which have to be made in the model in order to account for the average stress condition (4.46) are detailed in the Appendix Appendix A.3. Regarding the finite element calculations, the method used to impose the average stress while satisfying the condition of a uniform strain-rate on the boundary is described in Michel et al. (1999). Briefly, in this method the velocity field solution is decomposed in the form $\dot{\boldsymbol{u}} = \dot{\boldsymbol{E}}^i.\boldsymbol{x} + \dot{\boldsymbol{u}}'$, where both the fluctuating velocity field $\dot{\boldsymbol{u}}'$ and the macroscopic strain-rate $\dot{\boldsymbol{E}}^i$ are unknown. In order to impose the given macroscopic stress $\boldsymbol{\Sigma}^i$, a variational system on $\dot{\boldsymbol{u}}'$ and $\dot{\boldsymbol{E}}^i$ is written in which the components of the macroscopic stress appear as the generalized forces associated with $\dot{\boldsymbol{E}}^i$. The condition of a uniform strain-rate on the boundary is satisfied by imposing $\dot{\boldsymbol{u}}' = 0$ on ∂V. Both for the model and for the finite element calculations, the value of the macroscopic stress potential is determined as follows:

$$\widetilde{\Psi}(\boldsymbol{\Sigma}^i, p_l) = \frac{1}{n+1}\left(\boldsymbol{\Sigma}^i : \dot{\boldsymbol{E}}^i - p_l \frac{1}{|V|}\int_{\partial L} \dot{\boldsymbol{u}}.\boldsymbol{n}\, \mathrm{d}s\right). \tag{4.47}$$

We now specify the loading paths considered in the macroscopic stress space. The tensor $\boldsymbol{\Sigma}^0$ can be written in the following form, with respect to its principal axes:

$$\begin{pmatrix} \Sigma_1^0 \\ \Sigma_2^0 \\ \Sigma_3^0 \end{pmatrix} = \Sigma_m^0 \boldsymbol{i} + \frac{2}{3}\Sigma_{eq}^0 \begin{pmatrix} -\cos(\theta + \frac{\pi}{3}) \\ -\cos(\theta - \frac{\pi}{3}) \\ \cos(\theta) \end{pmatrix}, \tag{4.48}$$

where $\Sigma_m^0 = \mathrm{tr}\left(\boldsymbol{\Sigma}^0\right)/3$ and $\Sigma_{eq}^0 = (\frac{3}{2}\boldsymbol{\Sigma}^{0d} \cdot \boldsymbol{\Sigma}^{0d})^{\frac{1}{2}}$ are the first two isotropic invariants of $\boldsymbol{\Sigma}^0$, while θ is the Lode angle related to the third isotropic invariant of $\boldsymbol{\Sigma}^0$, $\det(\boldsymbol{\Sigma}^{0d}) = \frac{2}{27}{\Sigma_{eq}^0}^3 \cos(3\theta)$ (see for instance Danas et al. (2008)). To reduce the computational cost of the finite element simulations, attention is restricted to axisymmetric loading paths, *i.e.*, loading paths for which $\cos(\theta + \pi/3) = \cos(\theta - \pi/3)$. This does not affect the predictions of the model because with the secant approch used, the macroscopic stress potential predicted by the model depends on $\boldsymbol{\Sigma}^0$ only through its first two isotropic invariants Σ_m^0 and Σ_{eq}^0. However, the results of the finite element calculation can depend a priori on all three invariants of $\boldsymbol{\Sigma}^0$ (*i.e.*, on Σ_m^0, Σ_{eq}^0 and θ). The finite element calculations are therefore conducted on the two axisymmetric loading paths corresponding to the two Lode angles $\theta = 0$ and $\theta = \pi$.

Figure 3 shows the meshes used in the finite element calculations. Eight node quadratic axisymmetric elements with 2x2 Gauss points are used here and three different volume fractions of large voids are studied, namely, $f_l = 0.7\%$, 7%, and 14%. The three corresponding meshes contain 11587, 6309 and 4671 nodes, respectively. These discretizations have been found adequate for the accuracy of the finite element calculations, since further mesh refinement does not make any appreciable difference to the results.

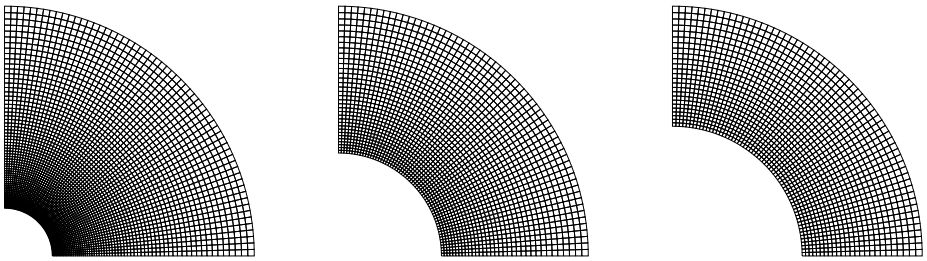

(a) (b) (c)

Figure 3: Meshes used in the finite element calculations (eight node quadratic elements). (a) $f_l = 0.7\%$, (b) $f_l = 7\%$, (c) $f_l = 14\%$.

4.2. Influence of the number of layers

Before comparing the results obtained with the finite element calculations, it is convenient to assess the effect of the number N of discretization layers on the predictions of the model. Apart from the linear case ($n = 1$ in (4.42)), where the exact solution can be obtained by taking a single layer in the porous matrix, the predictions of the model depend on the number of layers considered for the discretization of the porous matrix. The present study focuses on the case of high nonlinearity, where $n = 8$, and moderate porosities, $f_l = 7\%$ and $f_s = 5\%$. No internal pressures are assumed to exist in the voids, $p_l = p_s = 0$. Figure 4 shows the macroscopic equipotential surfaces obtained with these parameters with N=1, 2, 3, 5, 10 and 250 layers of the same thickness. In Figure 5, the corresponding macroscopic dimensionless mean and equivalent strain-rates, $\dot{E}_m/\dot{\varepsilon}_0$ and $\dot{E}_{eq}/\dot{\varepsilon}_0$, are plotted as a function of the macroscopic stress triaxiality $X = \Sigma_m/\Sigma_{eq}$. As can be seen in these two figures, the number of layers has low effect in the case of deviatoric loadings ($X \to 0$) but the effects are more pronounced at high stress triaxialities. Nevertheless, it can be observed that convergence is quickly reached, and that with the three different macroscopic quantities plotted in these two figures, $N = 10$ gives a good compromise between accuracy and computational cost at all stress triaxialities.

4.3. Comparison with finite element calculations

Once an appropriate number of layers have been adopted for the discretization of the porous matrix, the predictions of the model depend on several parameters: the nonlinearity exponent n, the volume fraction of the small and large voids, f_s and f_l, respectively, and the internal pressure in the large voids, p_l (as discussed above, the small voids can be taken to be stress-free here). Figures 6 and 7 show the influence of each of these parameters on the macroscopic equipotential surfaces.

Some general comments on these two figures can first be made. The macroscopic equipotential surfaces predicted by the model are always exterior to those obtained by the finite element calculations, which is consistent with the variational property $(4.40)_2$ of the macroscopic stress potential, since the local stress fields given by the model are statically admissible stress fields for the nonlinear problem. The predictions of the model were found to be always in excellent agreement with the finite element calculations at

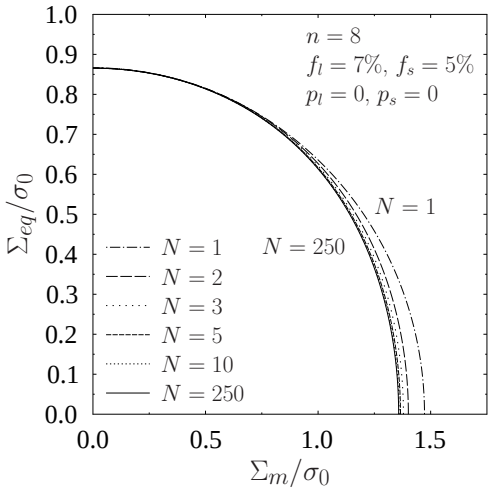

Figure 4: Macroscopic equipotential surfaces. Influence of the number N of layers on the predictions of the model. $n = 8$, $f_l = 7\%$, $f_s = 5\%$, $p_l = p_s = 0$.

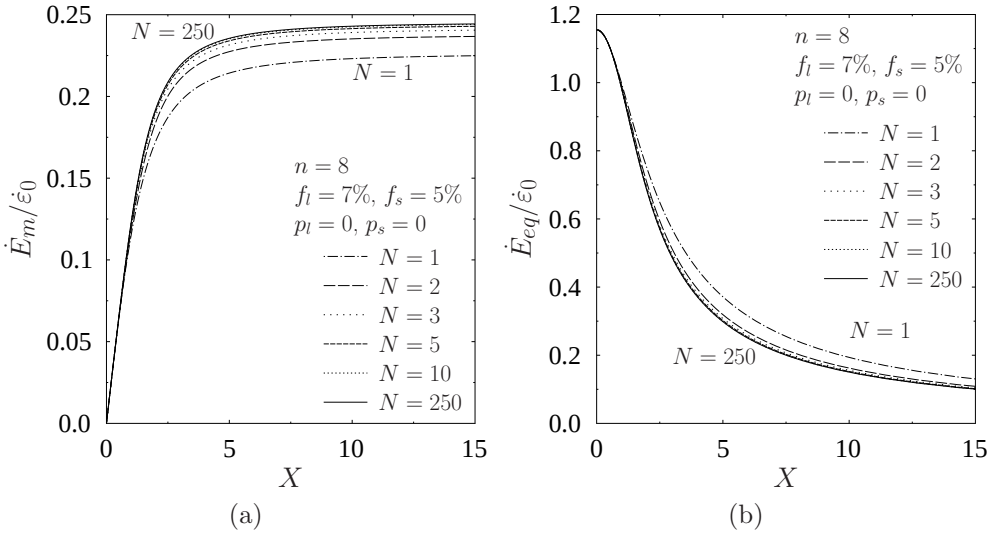

Figure 5: Macroscopic dimensionless mean (a) and equivalent (b) strain-rates, $\dot{E}_m/\dot{\varepsilon}_0$ and $\dot{E}_{eq}/\dot{\varepsilon}_0$, as a function of the macroscopic stress triaxiality $X = \Sigma_m/\Sigma_{eq}$. Influence of the number N of layers on the predictions of the model. $n = 8$, $f_l = 7\%$, $f_s = 5\%$, $p_l = p_s = 0$.

high stress triaxialities ($\Sigma_{eq} \to 0$), owing to the fact that the velocity field solution of the nonlinear problem is radial under purely hydrostatic loading conditions. In this case, regardless of the values of the parameters involved, the model is able to reproduce the exact result (as long as the number of layers is sufficiently large).

In Figure 6a, the volume fraction of the small and large voids is taken to be equal to $f_s = 5\%$ and $f_l = 7\%$, respectively, the voids are not pressurized ($p_l = p_s = 0$), and the macroscopic equipotential surfaces are plotted with three different nonlinearity exponent values: $n = 1$, 3 and 8. As mentioned in the previous section, in the case where $n = 1$ (the linear case), the predictions of the model are exact and the exact solution can even be obtained by considering only one layer in the matrix. For moderate and high nonlinearities, $n = 3$ and $n = 8$, respectively, the model predictions slightly overestimate the finite element results at moderate and low triaxialities. This difference was more pronounced at moderate triaxialities and increased with the nonlinearity. Note also the existence of a small difference between the finite element calculation results, depending on the value of the Lode angle θ (equal to 0 or π), which also increases with the nonlinearity.

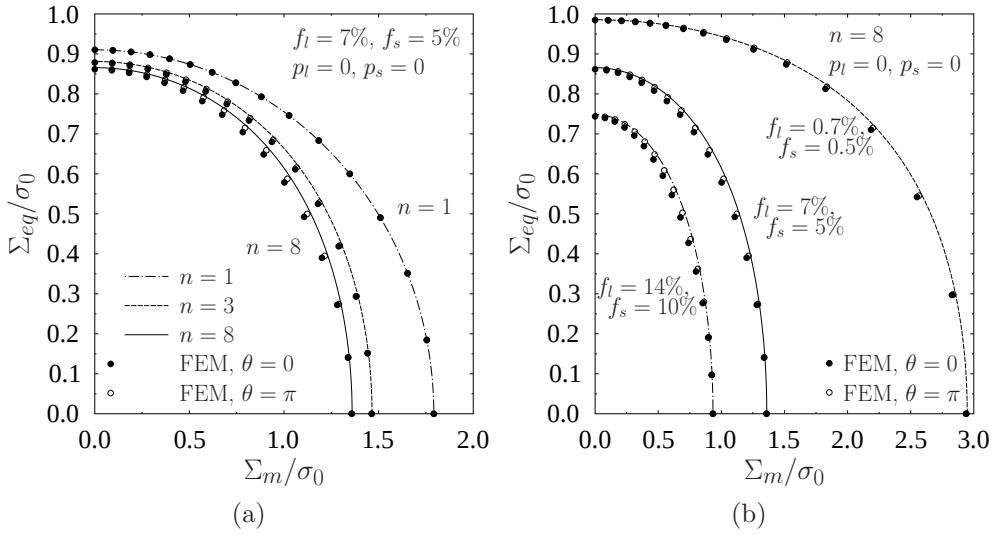

Figure 6: Influence of the nonlinearity exponent n (a) and the void volume fractions f_s and f_l (b) on the macroscopic equipotential surfaces. Comparison between the model predictions and the finite element calculation results. Non pressurized voids ($p_l = p_s = 0$). (a) $n = 1$, 3 and 8, $f_l = 7\%$, $f_s = 5\%$. (b) $n = 8$, $f_l = 0.7\%$, 7% and 14% with $f_s = 0.5\%$, 5% and 10%, respectively. Results based on the finite element calculations are marked with black filled circles (Lode angle $\theta = 0$) and white circles (Lode angle $\theta = \pi$), whereas the results based on the N-layer model are given by lines. $N = 20$ when $f_l = 0.7\%$, $N = 10$ when $f_l = 7\%$, 14%.

In Figure 6b, the macroscopic equipotential surfaces corresponding to different volume fractions f_s and f_l of the small and large voids are plotted in the case of high nonlinearity, $n = 8$, and non pressurized voids. Three ranges of porosities are considered: one corresponding to moderate porosity values, $f_l = 7\%$ and $f_s = 5\%$, as well as two others extreme cases corresponding to small and large porosities, $f_l = 0.7\%$, $f_s = 0.5\%$ and $f_l = 14\%$, $f_s = 10\%$, respectively. Again, the predictions of the model overestimate but

they were only slightly higher than the results obtained with the finite element method. Note that the difference between the finite element results corresponding to the two Lode angles $\theta = 0$ and $\theta = \pi$ increased with the void volume fractions, especially at moderate stress triaxialities.

The case presented in Figure 7 is that of a high nonlinearity, $n = 8$, with $f_l = 7\%$ and $f_s = 5\%$. The small voids are not pressurized. The macroscopic equipotential surfaces are plotted in this figure with three different values of the internal pressure in the large voids: $p_l = 0$, $0.75\sigma_0$ and $1.5\sigma_0$. Positive and negative stress triaxialities are both considered.

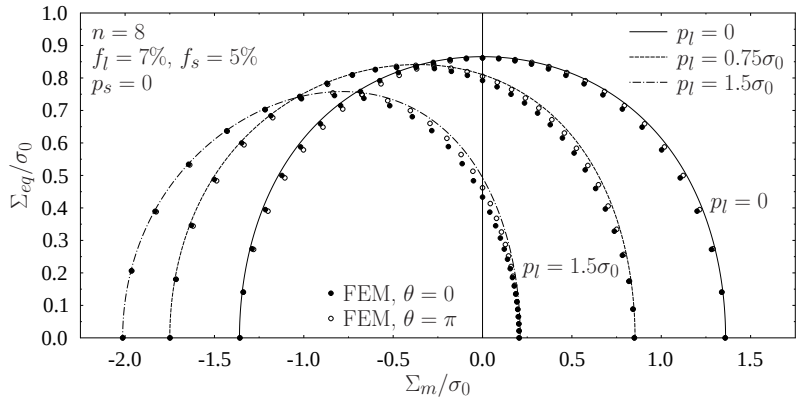

Figure 7: Influence of the internal pressure in the large voids, p_l, on the macroscopic equipotential surfaces. Comparison between the model predictions and the finite element calculation results. $n = 8$, $f_l = 7\%$, $f_s = 5\%$, $p_s = 0$, $p_l = 0$, $0.75\sigma_0$ and $1.5\sigma_0$. Results based on the finite element calculations are marked with black filled circles (Lode angle $\theta = 0$) and white circles (Lode angle $\theta = \pi$), whereas the results based on the N-layer model are given by lines. $N = 10$.

In the case where the large voids are not pressurized ($p_l = 0$), the macroscopic equipotential surface predicted by the model is symmetric with respect to the Σ_{eq}-axis. The corresponding macroscopic equipotential surfaces obtained by the finite element calculations with the two Lode angles $\theta = 0$ and $\theta = \pi$ differed and neither of them is symmetric because of the effects of the third invariant of the macroscopic stress on the macroscopic stress potential. However, in the case of non pressurized voids, since the macroscopic stress potential is an even function of the macroscopic stress, the part of the equipotential surface corresponding to $\theta = 0$ and $X > 0$ is the symmetric of the part of the equipotential surface corresponding to $\theta = \pi$ and $X < 0$, and conversely. When the large voids are pressurized ($p_l \neq 0$), neither the macroscopic equipotential surfaces predicted by the model nor those given by the finite element calculations are symmetric. In addition, the symmetry between the parts of the equipotential surfaces corresponding to the two Lode angles is lost.

As shown in Figure 7, increasing the internal pressure in the large voids has three main effects on the macroscopic equipotential surfaces. First, as discussed above, it changes the shape of the macroscopic equipotential surfaces. Secondly, it translates them along the Σ_m-axis, but not uniformly: the value of the translation depends on the internal pressure p_l as well as on the mean growth rate of the large voids (see expression (4.47)

for the macroscopic stress potential). Thirdly, the maximum value of the macroscopic equivalent stress decreases. Fairly good agreement was found to exist here between the predictions of the model and the finite element calculations. In addition, the differences between the different equipotential surfaces becomes blurred when the pressure in the large voids increases and the macroscopic mean stress decreases. For instance, in the case where $p_l = 1.5\sigma_0$, the macroscopic equipotential surface predicted by the model and those obtained with the two Lode angles differed for $-0.5\sigma_0 < \Sigma_m < 0.2\sigma_0$ and are superimposed when $\Sigma_m < -1.5\sigma_0$. This is due to the fact that imposing two sufficiently high pressures, one inside the large void and the other on the outer boundary of the representative volume element, leads to a local stress state which is almost hydrostatic. Therefore, in this case, the model can give almost the exact solution of the problem.

The results presented in Figures 8 and 10 correspond to the same parameters as in Figure 7. In Figure 8, the corresponding macroscopic mean and equivalent strain-rates are plotted as a function of the macroscopic stress triaxiality. The macroscopic strain-rate and the macroscopic equipotential surface are closely related: at a given point on the macroscopic equipotential surface, the corresponding macroscopic strain-rate is the outer normal at this point. When the voids are not pressurized, the macroscopic mean and equivalent strain-rates predicted by the model are odd and even functions of the macroscopic stress triaxiality, respectively. This is not the case in the finite element calculations, like for the macroscopic equipotential surfaces. Nonetheless, in the case of both non pressurized and pressurized large voids, the effect of the third invariant of the macroscopic stress is quite moderate and the macroscopic mean and equivalent strain-rates fairly accurately predicted by the model, especially at low and high triaxialities. In particular, as can be seen in Figure 8b, at low triaxialities, the vertex observed in the curves of the macroscopic equivalent strain-rate is very clearly accounted for by the model. At moderate triaxialities, the agreement between the predictions of the model and the finite element calculations is better for the macroscopic mean strain-rate than for the macroscopic equivalent strain-rate.

The curves plotted in Figure 8b could suggest that the macroscopic equivalent strain-rate do not asymptote to the same value at large positive and negative triaxialities. Figure 9 shows the macroscopic equivalent strain-rate, as a function of the inverse of the stress triaxiality, $1/X = \Sigma_{eq}/\Sigma_m$, for $X \to \pm\infty$. The results are plotted for small ($f_l = 0.7\%$, $f_s = 0.5\%$) moderate ($f_l = 7\%$, $f_s = 5\%$) and large ($f_l = 14\%$, $f_s = 10\%$) porosities and the same internal pressure in the large voids $p_l = 1.5\sigma_0$. In all cases the macroscopic equivalent strain-rate vanishes at purely hydrostatic loads ($X \to \pm\infty$) but it reaches zero more or less quickly. Note that for large porosities ($f_l = 14\%$, $f_s = 10\%$) the corresponding curves are both in the domain of negative triaxialities. This comes from the fact that for this range of porosities the effect of the internal pressure in the large voids on the macroscopic equipotential surface is to translate it entirely into the domain $\Sigma_m < 0$.

In applications, it is of interest to be able to estimate the void growth in a porous material. This process leads to the coalescence of the voids and potentially to the failure of the material by ductile fracture. Due to the incompressibility of the matrix phase at the microscopic scale, the mass balance gives:

$$\dot{f} = (1 - f)\,\mathrm{tr}\left(\dot{\boldsymbol{E}}\right), \tag{4.49}$$

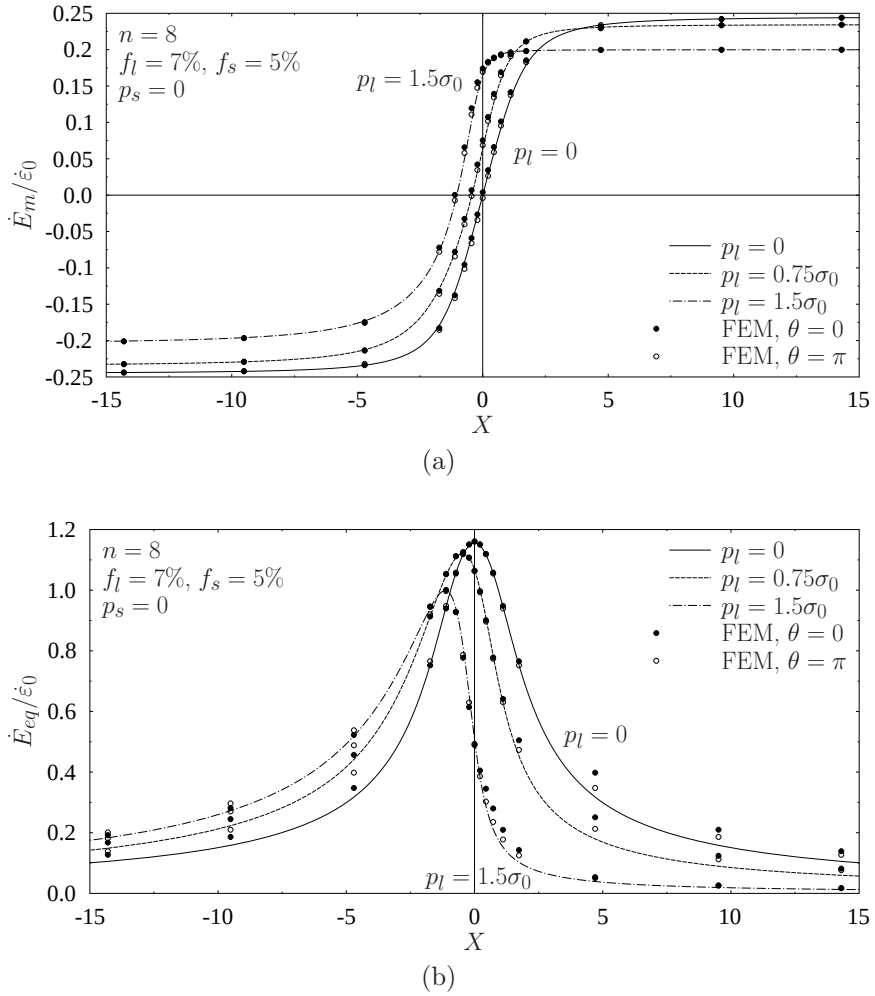

Figure 8: Influence of the internal pressure in the large voids, p_l, on the macroscopic dimensionless mean (a) and equivalent (b) strain-rates, $\dot{E}_m/\dot{\varepsilon}_0$ and $\dot{E}_{eq}/\dot{\varepsilon}_0$, as a function of the macroscopic stress triaxiality $X = \Sigma_m/\Sigma_{eq}$. Comparison between the model predictions and the finite element calculation results. $n = 8$, $f_l = 7\%$, $f_s = 5\%$, $p_s = 0$, $p_l = 0$, $0.75\sigma_0$ and $1.5\sigma_0$. Results based on the finite element calculations are marked with black filled circles (Lode angle $\theta = 0$) and white circles (Lode angle $\theta = \pi$), whereas results based on the N-layer model are given by lines. $N = 10$.

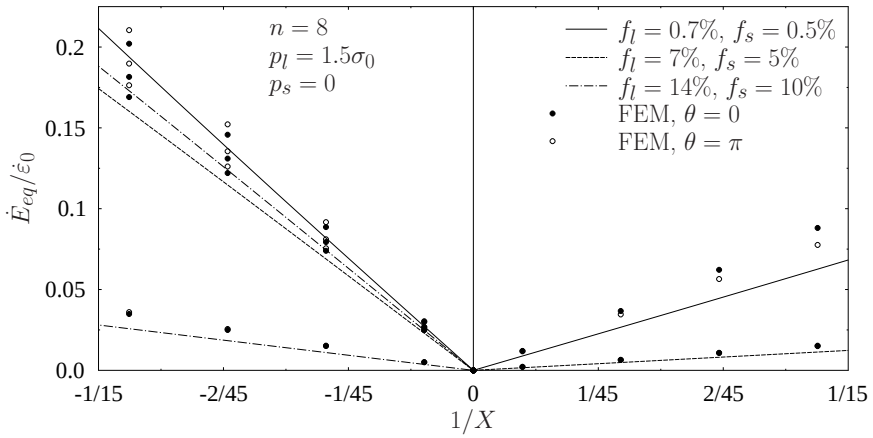

Figure 9: Macroscopic dimensionless equivalent strain-rate, $\dot{E}_{eq}/\dot{\varepsilon}_0$, as a function of the inverse of the macroscopic stress triaxiality, $1/X = \Sigma_{eq}/\Sigma_m$. Comparison between the model predictions and the finite element calculations for $n = 8$, $p_s = 0$, $p_l = 1.5\sigma_0$ and three ranges of porosities, $f_l = 0.7\%$, $f_s = 0.5\%$, $f_l = 7\%$, $f_s = 5\%$ and $f_l = 14\%$, $f_s = 10\%$. Results based on the finite element calculations are marked with black filled circles (Lode angle $\theta = 0$) and white circles (Lode angle $\theta = \pi$), whereas results based on the N-layer model are given by lines. $N = 20$ when $f_l = 0.7\%$, $N = 10$ when $f_l = 7\%$, 14%.

where f is the total porosity. Using (2.1), it follows by derivation with respect to time that:

$$\frac{\dot{\bar{f}}_s}{1-\bar{f}_s} + \frac{\dot{f}_l}{1-f_l} = \operatorname{tr}\left(\dot{\boldsymbol{E}}\right). \tag{4.50}$$

Owing to the compressibility of the porous matrix at the mesoscopic scale, the growth rate of the large voids is given by:

$$\dot{f}_l = \frac{1}{|V|}\int_{\partial L} \dot{\boldsymbol{u}}\cdot\boldsymbol{n}\,\mathrm{d}s - f_l \operatorname{tr}\left(\dot{\boldsymbol{E}}\right), \tag{4.51}$$

where $\boldsymbol{n}$ denotes the unit normal to ∂L pointing towards the porous matrix.

Figure 10 shows the dimensionless growth rate of the large and small voids, $\dot{f}_l/\dot{\varepsilon}_0$ and $\dot{\bar{f}}_s/\dot{\varepsilon}_0$, as a function of the macroscopic stress triaxiality. As can be seen in this figure, the void growth rates are very accurately predicted by the model at all stress triaxialities and with all three internal pressure values considered in the large voids. In the case where the large voids are not taken to be pressurized, the model and the finite element results have similar symmetry properties to those discussed above in connection with the previous figures. Increasing the internal pressure in the large voids (from 0 to $1.5\sigma_0$) has almost no effect on the growth rate of the small voids at small and negative macroscopic stress triaxialities, but it significantly affects this parameter at positive and high macroscopic stress triaxialities. As was to be expected, the internal pressure in the large voids is found to have significant effects on the growth rate of the large voids themselves at all the macroscopic stress triaxialities.

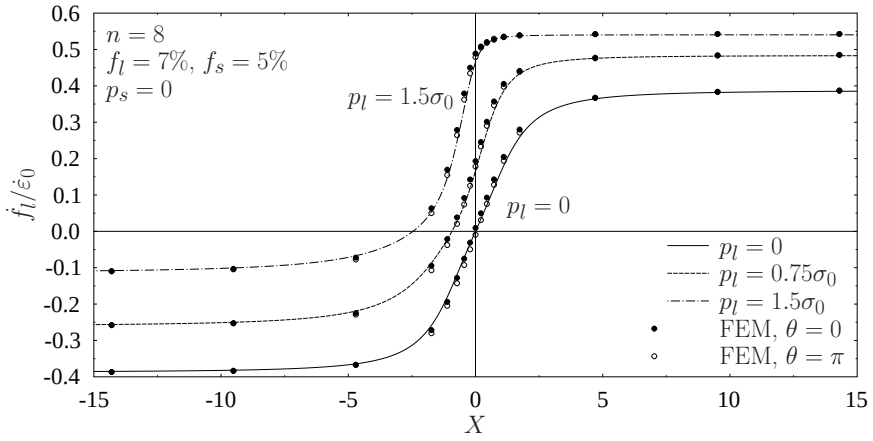

(a)

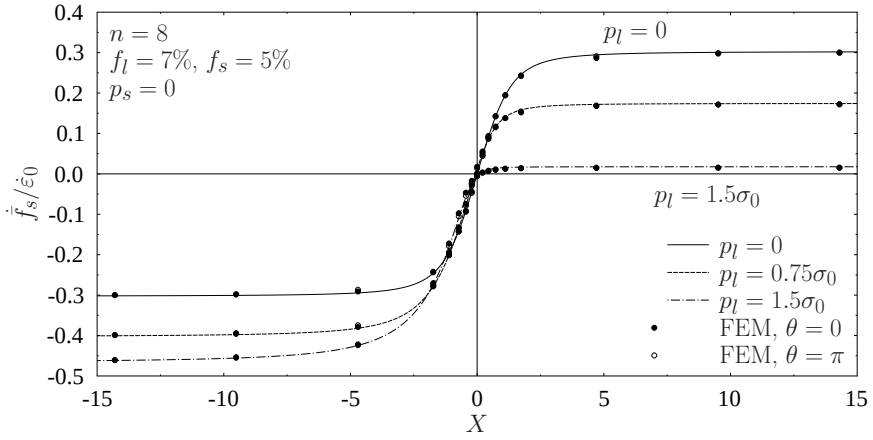

(b)

Figure 10: Influence of the internal pressure in the large voids, p_l, on the dimensionless growth rate of the large (a) and small (b) voids, $\dot{f}_l/\dot{\varepsilon}_0$ and $\dot{\bar{f}}_s/\dot{\varepsilon}_0$, as a function of the macroscopic stress triaxiality $X = \Sigma_m/\Sigma_{eq}$. Comparison between the model predictions and the finite element calculation results. $n = 8$, $f_l = 7\%$, $f_s = 5\%$, $p_s = 0$, $p_l = 0$, $0.75\sigma_0$ and $1.5\sigma_0$. Results based on the finite element calculations are marked with black filled circles (Lode angle $\theta = 0$) and white circles (Lode angle $\theta = \pi$), whereas those based on the N-layer model are given by lines. $N = 10$.

5. Conclusions

A micromechanical model for porous viscoplastic materials containing two populations of pressurized voids of different sizes is presented in this paper. The porous material is taken to be a three-scale composite comprising a microscopic scale corresponding to the size of the small voids, a mesoscopic scale corresponding to the size of the large voids, and a macroscopic scale.

The porous matrix at the mesoscopic scale is taken to be homogeneous and compressible. Its behavior derives from the potential(2.11-2.16), which was initially obtained by Michel and Suquet (1992) and modified in order to account for the pressure in the small voids.

The present study focuses on the second step in the homogenization procedure, which yields the proposed micromechanical model. The characteristics of the model are as follows:

- The macroscopic response is obtained using a simplified representative volume element: a hollow sphere containing a pressurized (large) void surrounded by a nonlinear viscoplastic compressible matrix.

- The nonlinearity of the matrix is approached using a modified secant linearization procedure involving the discretization of the hollow sphere into concentric layers having uniform secant moduli. A small number of layers (10 to 20 depending on the size of the central void) suffice to obtain accurate results.

- The approach used here is almost analytical. The part of the model which is treated numerically consists in solving a small linear system with about 60 unknowns.

The predictions of the model are assessed by comparing them with more accurate numerical results obtained using the finite element method. The model depends on several parameters, namely the volume fraction and the internal pressure of the small and large voids, and the nonlinearity exponent of the matrix phase. The influence of each of these parameters on the predictions of the effective behavior of the material is investigated. Good agreement is found to exist at all the macroscopic stress triaxialities and for all the porosity and nonlinearity values studied.

The model proposed here (coupled to others physical models) was used (Julien, 2008) in a qualification program, carried out by the French Commissariat à l'Énergie Atomique. The goal of this program is to investigate the incidental behavior of nuclear fuel used in pressurized water reactors. In order to simulate an incidental, in an experimental reactor the fuel rod is submitted to a sharp increase in the power (about twice the usual working power), and the power level reached is maintained for a few hours (so called a power ramp). Due to the high temperature reached (about 1800°C), during the power ramp (which lasts a few hours) the behaviour of the nuclear fuel can reasonably be considered as visco-plastic. This situation is very different from that of accidental one (studied by Vincent et al. (2009)), which lasts a few seconds or minutes. During such a short period of time the viscosity of the fuel plays no role.

The nuclear fuel is a porous polycrystalline material containing pressurized voids of different sizes, coming from the manufacture process (the pores) or generated during irradiation (the bubbles). The voids contain fission gases with different pressure levels.

It was observed experimentally (see Julien (2008) and references therein) that the pores and the bubbles differ in size, by a factor of 10 (or even more). Therefore, we can reasonably suppose that the material microstructure exhibits three scales corresponding to the bubbles size, pores size and the specimen size, respectively.

A recent study by Lebensohn et al. (2011) addresses the problem of macroscopic behaviour of viscoplastic polycrystalline materials containing intergranular voids. Using full-field numerical solutions obtained by FFT method, it is shown that crystallinity of the matrix material has a minor effect on the effective response. Thus, the matrix isotropy assumption, which is often made in theoretical studies, seems to be reasonable in the case where the polycrystal is macroscopically isotropic.

All these elements lead us to formulate the assumptions on which the present model is based.

Acknowledgements

The work by J. Julien was supported by a scholarship convention financed by Électricité de France. The work by M. Gărăjeu and J.-C. Michel was supported by the French Commissariat à l'Énergie Atomique via grant CEA-EDF-CNRS 3503001. The authors would like to acknowledge many discussions with Dr. R. Masson, partner of this study.

Bilger, N., Auslender, F., Bornert, M., Masson, R.. New bounds and estimates for porous media with rigid perfectly plastic matrix. Compte Rendu de l'Académie des Sciences 2002;:127–132.

Budiansky, B., Hutchinson, J., Slutsky, S.. Void growth and collapse in viscous solids. Mechanics of Solids: The Rodney Hill 60th Anniversary Volume 1982;:607 – 652.

Christensen, R.. Mechanics of Composite Materials. Malabar , Florida: Krieger Publishing Company, 1991.

Cocks, A.. Inelastic deformation of porous materials. J Mech Phys Solids 1989;**37**:693–715.

Danas, K., Idiart, M., Castañeda, P.P.. A homogenization-based constitutive model for isotropic viscoplastic porous media. International Journal of Solids and Structures 2008;**45**(11-12):3392 – 3409.

Duva, J., Hutchinson, J.. Constitutive potentials for dilutely voided non-linear materials. Mech Mater 1984;**3**:41–54.

Fabrègue, D., Pardoen, T.. A constitutive model for elastoplastic solids containing primary and secondary voids. Journal of the Mechanics and Physics of Solids 2008;56(3):719 – 741.

Gărăjeu, M., Michel, J., Suquet, P.. A micromechanical approach of damage in visco-plastic materials by evolution in size, shape and distribution of voids. Computer Methods in Applied Mechanics and Engineering 2000;**183**:223–246.

Gurson, A.. Continuum theory of ductile rupture by void nucleation and growth: Part i - yield criteria and flow rules for porous ductile media. J Eng Mat Tech 1977;**99**:2–15.

Hervé, E., Zaoui, A.. n-layered inclusion-based micromechanical modelling. Int J Engng Sci 1993;**31**(1):1–10.

Idiart, M.. Modeling the macroscopic behavior of two-phase nonlinear composites by infinite-rank laminates. J Mech Phys Solids 2008;**56**:2599–2617.

Julien, J.. Modélisation multi-échelles du couplage physico-chimie - mécanique du comportement du combustible à haute température des réacteurs à eau sous pression. Ph.D. thesis; Université de Provence; 2008.

Lebensohn, R., Idiart, M., Ponte Castañeda, P., Vincent, P.G.. Dilatational viscoplasticity of polycrystalline solids with intergranular cavities. to appear in Philosophical Magazine 2011;.

Leblond, J., Perrin, G., Suquet, P.. Exact results and approximate models for porous viscoplastic solids. International Journal of Plasticity 1994;**10**(3):213–235.

Michel, J., Moulinec, H., Suquet, P.. Effective properties of composite materials with periodic microstructure: a computational approach. Computer Methods in Applied Mechanics and Engineering 1999;**172**(1-4):109–143.

Michel, J., Suquet, P.. The constitutive law of nonlinear viscous and porous materials. J Mech Phys Solids 1992;**40**:783 – 812.

Nebozhyn, M.V., Ponte Castañeda, P.. The second-order procedure: exact vs approximate results for

isotropic, two-phase composites. Journal of the Mechanics and Physics of Solids 1999;**47**(10):2171 – 2185.
Pastor, J., Ponte Castañeda, P.. Yield criteria for porous media in plane strain: second-order estimates versus numerical results. Comptes Rendus Mécanique 2002;**330**(11):741 – 747.
Perrin, G., Leblond, J.. Analytical study of a hollow sphere made of plastic porous material and subjected to hydrostatic tension. application to some problems in ductile fracture of metals. Int J Plasticity 1990;**6**:677–699.
Ponte Castañeda, P.. The effective mechanical properties of nonlinear isotropic composites. J Mech Phys Solids 1991;**39**:45–71.
Ponte Castañeda, P.. New variational principles in plasticity and their application to composite materials. J Mech Phys Solids 1992;**40**(8):1757–1788.
Ponte Castañeda, P.. Exact second-order estimates for the effective mechanical properties of nonlinear composite materials. Journal of the Mechanics and Physics of Solids 1996;**44**(6):827–862.
Ponte Castañeda, P.. Second-order homogenization estimates for nonlinear composites incorporating field fluctuations. i. theory. J Mech Phys Solids 2002;**50**:737–757.
Sofronis, P., McMeeking, R.. Creep in power-law material containing spherical voids. J Appl Mech 1992;**59**:S88–S95.
Suquet, P.. On bounds for the overall potential of power law materials containing voids with an arbitrary shape. Mech Res Comm 1992;**19**(1):51–58.
Suquet, P.. Overall potentials and extremal surfaces of power law or ideally plastic composites. J Mech Phys Solids 1993;**41**:981–1002.
Suquet, P.. Overall properties of nonlinear composites : a modified secant moduli theory and its link with ponte castañeda's nonlinear variational procedure. Compte Rendu de l'Académie des Sciences Paris II 1995;**317**:1512–1522.
Vincent, P., Monerie, Y., Suquet, P.. Porous materials with two populations of voids under internal pressure. i. instantaneous constitutive relations. International Journal of Solids and Structures 2009;**46**:480–506.
Willis, J.. On methods for bounding the overall properties of nonlinear composites. J Mech Phys Solids 1991;**39**:73–86.

Appendix A. The systems of equations for the hollow sphere model

The system of equations for the coefficients A_i, B_i, C_i, D_i, F_i and G_i can be split into two systems corresponding to two types of boundary conditions: hydrostatic boundary conditions (when the macroscopic strain-rate tensor is spherical) and shear boundary conditions (when the macroscopic strain-rate tensor is deviatoric).

Appendix A.1. The case of hydrostatic boundary conditions

In the case of hydrostatic boundary conditions, the system of equations concerns the coefficients F_i and G_i. It is obtained using the continuity of the velocity field $\dot{\boldsymbol{u}}_1$ and the stress vector $\boldsymbol{\sigma}\cdot\boldsymbol{n}$ at the interfaces between layers:

$$\dot{u}^{(i)}(r_i) = \dot{u}^{(i+1)}(r_i), \quad \boldsymbol{\sigma}^{(i)}(r_i)\cdot\boldsymbol{e}_r = \boldsymbol{\sigma}^{(i+1)}(r_i)\cdot\boldsymbol{e}_r, \quad i = 1,..,N-1, \tag{A.1}$$

and the boundary conditions $(3.30)_1$:

$$\boldsymbol{\sigma}^{(1)}(r_0)\cdot\boldsymbol{e}_r = -p\,\boldsymbol{e}_r, \quad \dot{u}^{(N)}(r_N) = \dot{E}_m r_N. \tag{A.2}$$

Using the constitutive equations $(3.28)_1$ and the general form (3.32) of the velocity fields, it follows that the local stress fields in each layer i are diagonal in the basis of spherical coordinates (r,θ,φ). This gives:

$$\boldsymbol{\sigma}^{(i)}(r)\cdot\boldsymbol{e}_r = \sigma_{rr}^{(i)}(r)\,\boldsymbol{e}_r, \quad \sigma_{rr}^{(i)}(r) = 3k_iF_i - \frac{4\mu_i}{r^3}G_i, \quad i = 1,..,N.$$

Then the system of equations is:

$$\left\{\begin{array}{rcl} 3k_1F_1 - \frac{4\mu_1}{r_0^3}G_1 & = & -p, \\ F_i r_i + \frac{G_i}{r_i^2} - F_{i+1}r_i - \frac{G_{i+1}}{r_i^2} & = & 0, \quad i = 1, .., N-1, \\ 3k_iF_i - \frac{4\mu_i}{r_i^3}G_i - 3k_{i+1}F_{i+1} + \frac{4\mu_{i+1}}{r_i^3}G_{i+1} & = & 0, \quad i = 1, .., N-1, \\ F_N + \frac{G_N}{r_N^3} & = & \dot{E}_m. \end{array}\right. \tag{A.3}$$

Remark. The approach used here can be extended to the more general case where the small voids are pressurized with different internal pressures in each layer i. Let $p_s^{(i)}$ denote the internal pressure in the small voids of the layer i. The behavior of the porous matrix derives from a dissipation potential of the form (2.16). The first equation in (3.28) therefore becomes:

$$\boldsymbol{\sigma} = 3k_i\,\dot{\varepsilon}_m\,\boldsymbol{i} + 2\mu_i\,\dot{\boldsymbol{\varepsilon}}^d - p_s^{(i)}\boldsymbol{i} \quad \text{in } V^{(i)}.$$

This affects the first and the third equation in (A.3), which become:

$$\begin{array}{rcl} 3k_1F_1 - \frac{4\mu_1}{r_0^3}G_1 & = & p_s^{(1)} - p, \\ 3k_iF_i - \frac{4\mu_i}{r_i^3}G_i - 3k_{i+1}F_{i+1} + \frac{4\mu_{i+1}}{r_i^3}G_{i+1} & = & p_s^{(i)} - p_s^{(i+1)}, \quad i = 1, .., N-1. \end{array}$$

Appendix A.2. The case of shear boundary conditions

In the case of shear boundary conditions, the macroscopic strain-rate tensor is deviatoric, $\dot{\boldsymbol{E}} = \dot{\boldsymbol{E}}^d = \dot{\beta}\boldsymbol{\Delta}_{12} + \dot{\gamma}\boldsymbol{\Delta}_{13}$. The velocity field solution of (3.28) is given by the sum $\dot{\boldsymbol{u}}_2 + \dot{\boldsymbol{u}}_3$, where $\dot{\boldsymbol{u}}_2(\boldsymbol{x}) = \dot{\beta}\boldsymbol{\Delta}_{12}\cdot\boldsymbol{x}$ and $\dot{\boldsymbol{u}}_3(\boldsymbol{x}) = \dot{\gamma}\boldsymbol{\Delta}_{13}\cdot\boldsymbol{x}$ on ∂V. According to the definition of the deviatoric tensors $\boldsymbol{\Delta}_{12}$ and $\boldsymbol{\Delta}_{13}$, if the components of $\dot{\boldsymbol{u}}_2$ in the Cartesian basis are $\dot{u}_x$, $\dot{u}_y$ and $\dot{u}_z$, then the components of $\dot{\boldsymbol{u}}_3$ in that same basis will be $\dot{u}_x$, $\dot{u}_z$ and $\dot{u}_y$. Therefore, both fields $\dot{\boldsymbol{u}}_2$ and $\dot{\boldsymbol{u}}_3$ depend on the same functions $U(r)$ and $V(r)$ and on the same set of coefficients A_i, B_i, C_i and D_i. The system of equations is obtained using the continuity of the velocity field $\dot{\boldsymbol{u}}_2$ and the stress vector $\boldsymbol{\sigma}\cdot\boldsymbol{n}$ at the interfaces between layers:

$$\begin{array}{c} U^{(i)}(r_i) = U^{(i+1)}(r_i), \quad V^{(i)}(r_i) = V^{(i+1)}(r_i), \\ \boldsymbol{\sigma}^{(i)}(r_i,\,\theta,\,\varphi)\cdot\boldsymbol{e}_r = \boldsymbol{\sigma}^{(i+1)}(r_i,\,\theta,\,\varphi)\cdot\boldsymbol{e}_r, \quad i = 1, .., N-1, \end{array} \tag{A.4}$$

and the boundary conditions $(3.30)_2$:

$$\boldsymbol{\sigma}^{(1)}(r_0,\,\theta,\,\varphi)\cdot\boldsymbol{e}_r = 0, \quad U^{(N)}(r_N) = r_N, \quad V^{(N)}(r_N) = r_N. \tag{A.5}$$

The resulting equations for the functions $U^{(i)}(r)$ and $V^{(i)}(r)$ can be readily written using the expressions (3.35). The other equations require calculating the stress vector, which, in the basis of spherical coordinates, is of the form:

$$\boldsymbol{\sigma}.\boldsymbol{e}_r = \sigma_{rr}\boldsymbol{e}_r + \sigma_{r\theta}\boldsymbol{e}_\theta + \sigma_{r\varphi}\boldsymbol{e}_\varphi.$$

Using the constitutive equations $(3.28)_1$ and the general form (3.33) of the velocity fields, it follows that there exist only two independent equations which express the continuity of the stress vector. At each interface $r = r_i$, $i = 1, .., N-1$:

$$\sigma_{rr}^{(i)}(r_i,\theta,\varphi) = \sigma_{rr}^{(i+1)}(r_i,\theta,\varphi), \quad \sigma_{r\theta}^{(i)}(r_i,\theta,\varphi) = \sigma_{r\theta}^{(i+1)}(r_i,\theta,\varphi), \quad \forall\,\theta,\varphi,$$

where

$$\sigma_{rr}^{(i)}(r,\,\theta,\,\varphi) = \left[2A_i\mu_i + B_i(3k_i - 2\mu_i)r^2 - \tfrac{24C_i\mu_i}{r^5} - 2D_i\tfrac{9k_i+4\mu_i}{r^3}\right]\sin^2\theta\cos 2\varphi,$$
$$\sigma_{r\theta}^{(i)}(r,\,\theta,\,\varphi) = \left[A_i\mu_i - B_i\left(8k_i + \tfrac{5}{3}\mu_i\right)r^2 + \tfrac{8C_i\mu_i}{r^5} + \tfrac{3D_ik_i}{r^3}\right]\sin 2\theta\cos 2\varphi.$$

There also exist only two independent equations which express the condition on the inner boundary $r = r_0$:

$$\sigma_{rr}^{(1)}(r_0,\,\theta,\,\varphi) = \sigma_{r\theta}^{(i)}(r_0,\,\theta,\,\varphi) = 0, \quad \forall\,\theta,\varphi.$$

Appendix A.3. The case of prescribed macroscopic stress

In the case where the macroscopic stress is prescribed, the average stress condition (4.46) yields the following local problem:

$$\begin{cases} \boldsymbol{\sigma} = 3k_i\,\dot{\varepsilon}_m\,\boldsymbol{i} + 2\mu_i\,\dot{\boldsymbol{\varepsilon}}^d \quad \text{in } V^{(i)}, \quad i = 1,..,N, \\ \operatorname{div}\boldsymbol{\sigma} = 0 \quad \text{in } V - L, \\ \boldsymbol{\sigma}.\boldsymbol{n} = -p\,\boldsymbol{n} \quad \text{on } \partial L, \\ \dot{\boldsymbol{u}} = \dot{\boldsymbol{E}}.\boldsymbol{x} \quad \text{on } \partial V, \quad \dot{\boldsymbol{E}} \text{ unknown}, \\ \frac{1}{|V|}\int_{\partial V}\boldsymbol{\sigma}.\boldsymbol{n}\otimes_s\boldsymbol{x}\,\mathrm{d}s = \boldsymbol{\Sigma}, \quad \boldsymbol{\Sigma} \text{ given}. \end{cases} \tag{A.6}$$

The question addressed in this section is how the systems of equations for the coefficients A_i, B_i, C_i, D_i, F_i and G_i should be changed?

The macroscopic stress and strain-rate tensors are related by $\dot{\boldsymbol{E}} = \frac{\partial\widetilde{\Psi}}{\partial\boldsymbol{\Sigma}}(\boldsymbol{\Sigma}, p)$. Therefore, when the macroscopic stress potential $\widetilde{\Psi}$ is an isotropic function of $\boldsymbol{\Sigma}$ (which is the case here), the macroscopic tensors $\boldsymbol{\Sigma}$ and $\dot{\boldsymbol{E}}$ have the same principal directions and in the basis of principal directions, they are both diagonal. Moreover, a null principal value for one tensor is also a principal value for the other tensor. The macroscopic stress tensor can be decomposed as follows:

$$\begin{gathered} \boldsymbol{\Sigma} = \boldsymbol{\Sigma}_1 + \boldsymbol{\Sigma}_2 + \boldsymbol{\Sigma}_3, \\ \boldsymbol{\Sigma}_1 = \Sigma_m\boldsymbol{i}, \quad \boldsymbol{\Sigma}_2 = \Theta\boldsymbol{\Delta}_{12}, \quad \boldsymbol{\Sigma}_3 = \omega\boldsymbol{\Delta}_{13}, \end{gathered} \tag{A.7}$$

where $\Theta\boldsymbol{\Delta}_{12}, +\omega\boldsymbol{\Delta}_{13} = \boldsymbol{\Sigma}^d$. It follows from the above mentioned result that the corresponding macroscopic strain-rate tensors can be written:

$$\dot{\boldsymbol{E}}_1 = \dot{E}_m\boldsymbol{i}, \quad \dot{\boldsymbol{E}}_2 = \dot{\beta}\boldsymbol{\Delta}_{12}, \quad \dot{\boldsymbol{E}}_3 = \dot{\gamma}\boldsymbol{\Delta}_{13}. \tag{A.8}$$

The velocity field solution of (A.6) is therefore the sum of the same three velocity fields (3.29). Their coefficients must satisfy the same systems of equations but the values of $\dot{E}_m$, $\dot{\beta}$ and $\dot{\gamma}$ are not known.

The system for the coefficients A_i, B_i, C_i and D_i (eqns (A.4-A.5)) does not depend on $\dot{\beta}$ and $\dot{\gamma}$ and can be solved independently. The average conditions

$$\frac{1}{|V|}\int_{\partial V}\boldsymbol{\sigma}.\boldsymbol{n}\otimes_s\boldsymbol{x}\,\mathrm{d}s = \boldsymbol{\Sigma}_2 \quad \text{and} \quad \frac{1}{|V|}\int_{\partial V}\boldsymbol{\sigma}.\boldsymbol{n}\otimes_s\boldsymbol{x}\,\mathrm{d}s = \boldsymbol{\Sigma}_3, \tag{A.9}$$

are then used to obtain $\dot{\beta}$ and $\dot{\gamma}$. Straightforward calculations yield the following expressions for the average conditions (A.9):

$$-\frac{2\left[7B_N(3k_N+\mu_N)r_N^5-5A_N\mu_N r_N^3+D_N(9k_N+8\mu_N)\right]}{5r_N^3}=\frac{\Theta}{\dot{\beta}}=\frac{\omega}{\dot{\gamma}}. \tag{A.10}$$

For the coefficients F_i and G_i, the system (A.3) depends on $\dot{E}_m$ (which is not known) and the average condition $\frac{1}{|V|}\int_{\partial V}\boldsymbol{\sigma}.\boldsymbol{n}\otimes_s\boldsymbol{x}\,\mathrm{d}s=\boldsymbol{\Sigma}_1$ should be added to the system. This average condition can be written as:

$$3F_Nk_N-\frac{4G_N\mu_N}{r_N^3}=\Sigma_m, \tag{A.11}$$

and (A.3) is replaced by the following system in which the unknowns are both the macroscopic mean strain-rate $\dot{E}_m$ and the coefficients F_i and G_i:

$$\left\{\begin{array}{rcl}
3k_1F_1-\frac{4\mu_1}{r_0^3}G_1 &=& -p,\\
F_ir_i+\frac{G_i}{r_i^2}-F_{i+1}r_i-\frac{G_{i+1}}{r_i^2} &=& 0,\quad \text{i=1,..,N-1,}\\
3k_iF_i-\frac{4\mu_i}{r_i^3}G_i-3k_{i+1}F_{i+1}+\frac{4\mu_{i+1}}{r_i^3}G_{i+1} &=& 0,\quad \text{i=1,..,N-1,}\\
F_N+\frac{G_N}{r_N^3}-\dot{E}_m &=& 0,\\
3F_Nk_N-\frac{4G_N\mu_N}{r_N^3} &=& \Sigma_m.
\end{array}\right. \tag{A.12}$$

Appendix B. Proof of Lemma 1

Using the divergence theorem, one obtains:

$$\int_{\Omega-S}\operatorname{div}\boldsymbol{v}\,\mathrm{d}\boldsymbol{x}=\int_{\partial S}\boldsymbol{v}\cdot\boldsymbol{n}\,\mathrm{d}s+\int_{\partial\Omega}\boldsymbol{v}\cdot\boldsymbol{n}\,\mathrm{d}s. \tag{B.1}$$

Since $\boldsymbol{v}(\boldsymbol{x})=\dot{\boldsymbol{\varepsilon}}\cdot\boldsymbol{x}$ on $\partial\Omega$, the last integral gives:

$$\int_{\partial\Omega}\boldsymbol{v}\cdot\boldsymbol{n}\,\mathrm{d}s=\int_{\partial\Omega}(\dot{\boldsymbol{\varepsilon}}\cdot\boldsymbol{x})\cdot\boldsymbol{n}\,\mathrm{d}s=\int_{\partial\Omega}\dot{\boldsymbol{\varepsilon}}\cdot(\boldsymbol{x}\otimes\boldsymbol{n})\,\mathrm{d}s=\dot{\boldsymbol{\varepsilon}}\cdot\int_{\partial\Omega}\boldsymbol{x}\otimes\boldsymbol{n}\,\mathrm{d}s.$$

Again using the divergence theorem, we obtain $\int_{\partial\Omega}\boldsymbol{x}\otimes\boldsymbol{n}\,\mathrm{d}s=|\Omega|\boldsymbol{i}$, and therefore:

$$\int_{\partial\Omega}\boldsymbol{v}\cdot\boldsymbol{n}\,\mathrm{d}s=|\Omega|\mathrm{tr}\left(\dot{\boldsymbol{\varepsilon}}\right). \tag{B.2}$$

Substituting (B.2) into (B.1) gives (2.14).